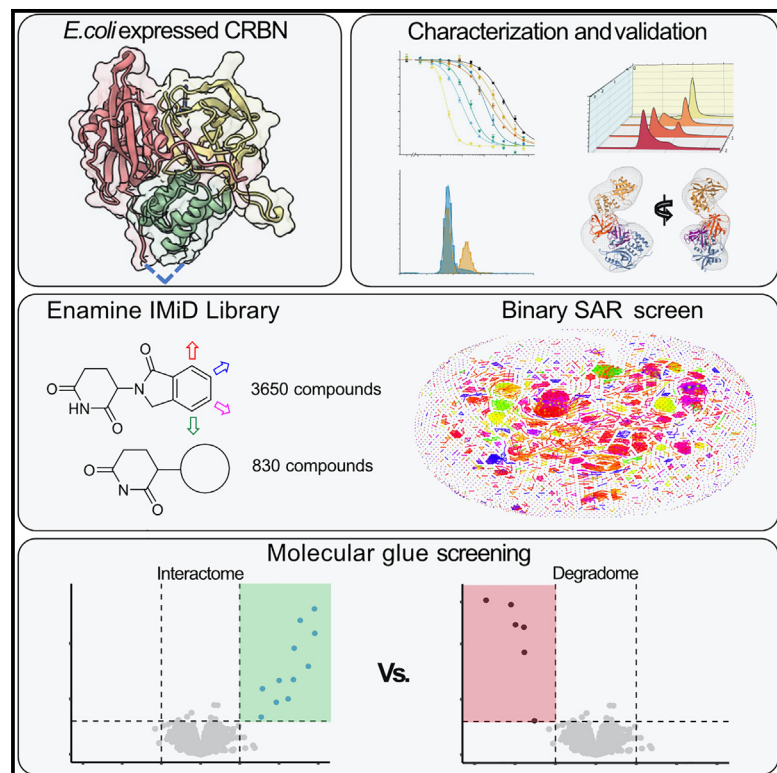


Cell Chemical Biology

An engineered cereblon optimized for high-throughput screening and molecular glue discovery

Graphical abstract



Authors

Henry J. Bailey, Jonathan Eisert, Rubina Kazi, ..., Radosław P. Nowak, Fiona J. Sorrell, Ivan Dikic

Correspondence

fiona.sorrell@merckgroup.com (F.J.S.), dikic@biochem2.uni-frankfurt.de (I.D.)

In brief

Due to challenges in studying molecular interactions of CRBN, identification of CRBN based molecular glues has remained underexplored. Here, Bailey et al designed an easy-to-handle CRBN construct and applied chemo-proteomics approaches for molecular glue discovery. Results unlock the hidden cellular interactomes of IMiD based molecular glues and PROTACs.

Highlights

- An engineered CRBN construct, CRBN_ΔHBD, is easy to handle and express in *E. coli*
- CRBN_ΔHBD is active in binary and ternary complex formation studies
- High-throughput screening methods allow SAR analysis of the Enamine IMiD library
- FLAG-CRBN_ΔHBD can determine cellular interactomes of molecular glues and PROTACs



Resource

An engineered cereblon optimized for high-throughput screening and molecular glue discovery

Henry J. Bailey,^{1,5,11} Jonathan Eisert,^{2,11} Rubina Kazi,¹ Jan Gerhartz,³ Dominika Ewa Pieńkowska,³ Ina Dressel,³ Joshua Vollrath,^{1,4,5} Ivan Kondratov,^{6,7,8} Tetiana Matviyuk,⁶ Nataliya Tolmachova,⁶ Varun Jayeshkumar Shah,¹ Giulio Giuliani,¹ Thorsten Mosler,¹ Thomas M. Geiger,³ Ana M. Esteves,⁹ Sandra P. Santos,⁹ Raquel L. Sousa,⁹ Tiago M. Bandejas,⁹ Eva-Maria Leibrock,² Ulrike Bauer,² Birgitta Leuthner,² Julian D. Langer,^{5,10} Ansgar A. Wegener,² Radosław P. Nowak,³ Fiona J. Sorrell,^{2,*} and Ivan Dikic^{1,5,12,*}

¹Institute of Biochemistry II, Medical Faculty, Goethe-University, Frankfurt am Main and Buchmann Institute for Molecular Life Sciences, Frankfurt am Main, Germany

²Merck Healthcare KGaA, Discovery and Development Technologies, Frankfurter Straße 250, 64293 Darmstadt, Germany

³Institute of Structural Biology, University of Bonn, Venusberg Campus 1, 53127 Bonn, Germany

⁴Max Planck Institute of Biophysics, IMPRS on Cellular Biophysics, Max-von-Laue-Strasse 3, 60439 Frankfurt am Main, Germany

⁵Max Planck Institute of Biophysics, Max-von-Laue-Strasse 3, 60439 Frankfurt am Main, Germany

⁶Enamine Ltd., Winston Churchill Street 78, 02094 Kyiv, Ukraine

⁷Enamine Germany GmbH, Industriepark Hoechst, G837, 65926 Frankfurt am Main, Germany

⁸V. P. Kukhar Institute of Bioorganic Chemistry and Petrochemistry, National Academy of Sciences of Ukraine, Akademik Kukhar Street 1, 02094 Kyiv, Ukraine

⁹iBET, Instituto de Biologia Experimental e Tecnológica, Apartado 12, 2781-901 Oeiras, Portugal

¹⁰Max Planck Institute for Brain Research, Max-von-Laue-Strasse 4, 60439 Frankfurt am Main, Germany

¹¹These authors contributed equally

¹²Lead contact

*Correspondence: fiona.sorrell@merckgroup.com (F.J.S.), dikic@biochem2.uni-frankfurt.de (I.D.)

<https://doi.org/10.1016/j.chembiol.2024.11.002>

SIGNIFICANCE The untapped potential for the discovery of molecular glue substrates leaves huge potential for exciting developments in this field. Through simplification of CRBN production and optimization of multiple biophysics and biochemical assays to measure ternary complex formation, we hope to provide improved resources for the validation and characterization of CRBN-based degraders. We show this applicability here through development of the “Enamine CRBN focused IMiD library” of 4480-IMiD based derivatives and application of our CRBN construct in high-throughput screening for the discovery of next generation binders. Importantly, our CRBN-based assays also extend to the cellular context allowing further assessment of CRBN binder interactomes by mass spectrometry providing exciting tools for target validation and specificity profiling. Taken together, we believe combining our IMiD based chemical binding landscape and “binding first” interactome screening approach with existing protein degradation profiling tools will have high potential to accelerate the future discovery of next generation CRBN glue substrates and degrader molecules.

SUMMARY

The majority of clinical degraders utilize an immunomodulatory imide drug (IMiD)-based derivative that directs their target to the E3 ligase receptor cereblon (CRBN); however, identification of IMiD molecular glue substrates has remained underexplored. To tackle this, we design human CRBN constructs, which retain all features for ternary complex formation, while allowing generation of homogenous and cost-efficient expression in *E. coli*. Extensive profiling of the construct shows it to be the “best of both worlds” in terms of binding activity and ease of production. We next designed the “Enamine focused IMiD library” and demonstrated applicability of the construct to high-throughput screening, identifying binders with high potency, ligand efficiency, and specificity. Finally, we adapt our construct for proof of principle glue screening approaches enabling IMiD cellular interactome determination. Coupled with our IMiD binding landscape the methods described here should serve as valuable tools to assist discovery of next generation CRBN glues.



INTRODUCTION

Targeted protein degradation (TPD) has emerged as an important therapeutic modality that utilizes bifunctional degrader molecules, such as proteolysis targeting chimeras (PROTACs) or molecular glues (MGs), to recognize and recruit specific proteins to E3 ligase complexes for ubiquitination and subsequent degradation via the cellular ubiquitin-proteasome system.^{1–3} The majority of PROTACs and MGs currently in clinical trials utilize an IMiD-based derivative, such as thalidomide, lenalidomide, or pomalidomide, that directs their target substrate to the E3 ligase receptor cereblon (CRBN), making CRBN the most successful effector protein within the TPD field.^{4–6} However, despite their success in treatments of cancer, IMiD molecules are known to be teratogenic, which limits their use to tightly controlled clinical scenarios and constrains development of PROTACs based on these binders.⁷ While the teratogenicity of IMiDs is linked to concomitant degradation of transcription factor SALL4, which genetic loss of function phenocopies the effect of IMiDs and has been misdiagnosed as thalidomide syndrome, the full spectrum of factors involved remains to be elucidated. Recent efforts have led to the exciting discovery of next generation IMiD scaffolds which aim to eliminate the undesirable off-target toxicity,⁸ allowing for the design of potent and specific PROTAC degraders entering clinical trials. IMiD molecular glues specifically target a structural glycine containing beta-hairpin motif, frequently called a “G-loop”, present in the C2H2 domain of many zinc finger transcription factors, such as SALL4. Beyond the canonical C2H2 zinc finger motif, IMiD based derivatives have been further shown to recruit a kinase (CK1 α)⁹ and GTPase (GSPT1)¹⁰ which contain just the minimal G-loop degron sequences, providing indications that other protein classes with this common motif could potentially be targeted through variation of the IMiD based chemistry and optimization of molecular glue screening assays.

CRBN is a substrate adapter protein which complexes with adapter protein DDB1 and CUL4 to form a CRL4^{CRBN} E3 ligase assembly. CRBN has a modular structure (Figure 1A) with an N-terminal Lon protease-like domain, an intermedial helical bundle domain (HBD) followed by a C-terminal thalidomide binding domain (TBD) that binds the glutarimide moiety of IMiDs within a tryptophan cage pocket.^{11–14} In addition to the ligand binding pocket, the TBD encodes a sensor loop that allows for conformational crosstalk between the TBD and Lon domain during compound binding.¹⁵ Second generation high affinity elaborations of the core IMiD scaffold, such as mezigdomide and iberdomide, harness this crosstalk through direct interactions with the sensor loop, favoring transition to a closed CRBN conformation that allows the Lon N domain to provide stabilizing interactions to the TBD pocket.¹⁵ In contrast, the helical bundle domain does not participate in ligand binding, instead it contributes 55 amino acids for recruiting the CUL4 ubiquitin ligase machinery via direct interaction with the adapter protein DDB1 (Figure 1A).^{12,14}

Two recombinant human CRBN constructs have been previously described for characterization of CRBN-based degraders; however, significant hurdles exist that limit their applicability for current biophysical and biochemical screening methods. The minimal TBD (CRBN_TBD) construct is expressed in *E. coli* cells but

lacks important contributions from the Lon N domain and the sensor loop which limits its activity and affinity during IMiD binding.^{15,16} A bacterial cereblon isoform from *Magnetospirillum gryphiswaldense* (MsCl4), designed to correspond to the human TBD region for high-throughput ligand screening, is also shown to bind ligands with affinities several orders of magnitude lower than reported for human full-length cereblon.¹⁷ Another, near full-length, human CRBN construct can also be purified using specialized and costly insect cell expression as a heterodimer with the interaction partner DDB1. Insect cell CRBN-DDB1 complex can be heterogeneous due to dissociation of the DDB1, presenting challenges for structural and biophysical assays and making a large scale screening efforts a costly endeavor.¹¹

To tackle this, we engineer an intermediate human CRBN construct (CRBN_ΔHBD), that contains all important structural regions for compound binding, and purify from a simple, convenient *E. coli* expression system. We develop several binary and ternary interaction assays and show highly desirable properties of CRBN_ΔHBD for the evaluation of PROTACs and molecular glues providing invaluable tools to delineate structure activity relationships of IMiD based degrader compounds in terms of binary and ternary complex formation.

Since the mechanism for all IMiD based degradation requires binding to CRBN, and diversification of the solvent exposed moiety leads to degradation of distinct protein substrates, we reason that (structure activity relationship) SAR information describing binary binding affinity can act as a starting point to prioritize diverse scaffolds which can then be assessed for their downstream degradation propensity and ternary complex formation properties. To achieve this, we optimize high-throughput ligand primary screening assays and partner these with a focused CRBN library of 4480-compounds supplied by Enamine to discover next generation CRBN binders with improved binary affinity, ligand efficiency, and specificity, indicating this construct will be valuable in the search for diverse CRBN binders. Finally, to gain insights into ternary complex formation we apply our CRBN construct for proof of principle co-immunoprecipitation (coIP) assays in mammalian cell lysates. We show strong enrichment of known IMiD dependent neosubstrates within the C2H2 zinc finger family and identify five putative binders of diverse protein families, which also contain the minimal G-loop degron motif. In conclusion, we present a CRBN_ΔHBD as a versatile reagent which can be used to not only identify potent chemical binders across the diverse IMiD chemical landscape but also the corresponding neosubstrate interactome in immunoprecipitation-mass spectrometry (IP-MS) experiments.

RESULTS

CRBN_ΔHBD can be expressed and purified from low cost *E. coli* expression system

We hypothesized the limiting factor preventing soluble full-length human CRBN production to be the exposure of several hydrophobic patches in the helical bundle domain (HBD) to solution in the absence of the binding partner DDB1. Inspection of the CRBN:DDB1 complex structure^{12,14} revealed the DDB1 interacting residues (aa 194–248) of the HBD could easily be deleted and replaced with a soluble GNGNSG linker to form an intermediate CRBN construct (CRBN_ΔHBD) (human residues 47–193 and

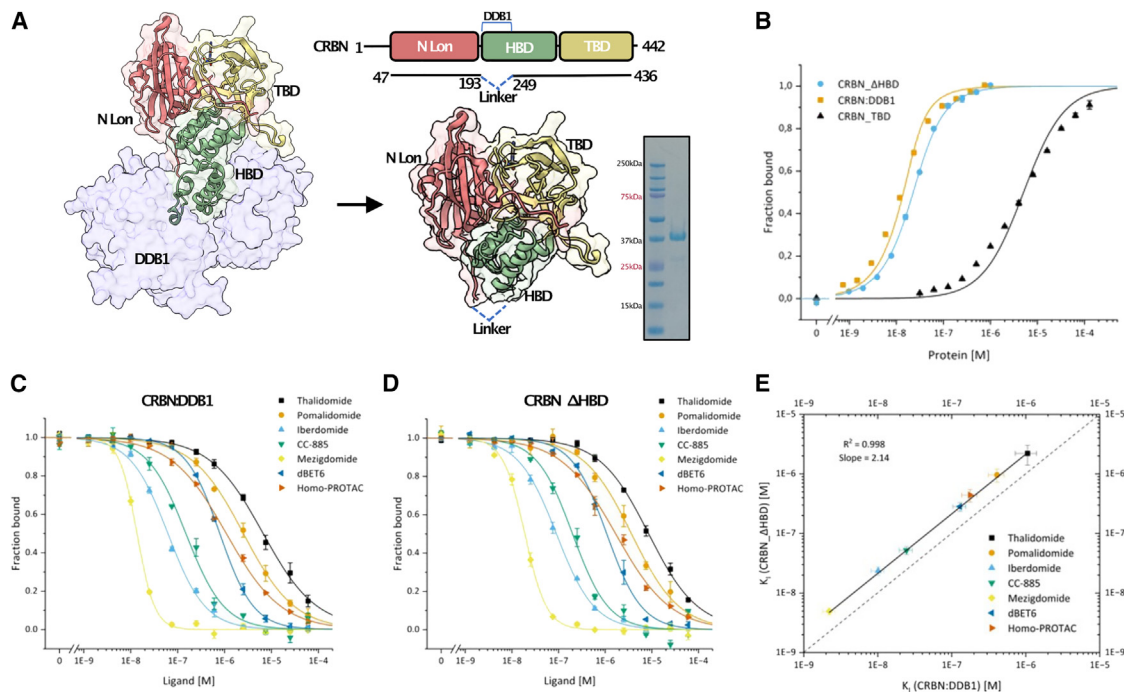


Figure 1. CRBN_ΔHBD retains binary tool compound affinity

(A) Linker design for expression and purification of soluble near full-length CRBN (CRBN_ΔHBD) in *E. coli*.

(B) Fluorescence polarization assay comparing affinity for thalidomide-based Cy5 tracer to CRBN_ΔHBD versus the minimal thalidomide binding domain (TBD) and CRBN:DDB1 complex. Data are presented as mean \pm SD ($n = 4$).

(C) Competitive fluorescence polarization assay comparing K_i of published tool CRBN PROTACs and molecular glues against CRBN:DDB1 complex. Data are presented as mean \pm SD ($n = 3$).

(D) Competitive fluorescence polarization assay comparing K_i of published tool CRBN PROTACs and molecular glues against CRBN_ΔHBD. Data are presented as mean \pm SD ($n = 3$).

(E) K_i correlations of tool CRBN compounds between CRBN_ΔHBD and the CRBN:DDB1 complex. Data are presented as mean \pm SD ($n = 3$).

249–436) (Figures 1A and Data S1). AlphaFold models show CRBN_ΔHBD can adopt the functional closed conformation with an root-mean-square deviation (RMSD) of 0.6 across 309 residues when overlaid with full-length CRBN (PDB: 6BOY)¹⁸ indicating the deletion of the DDB1 interacting sequence in CRBN does not perturb the structure of the TBD and Lon N domains (Figure S1A). MBP-His-CRBN_ΔHBD was expressed in *E. coli* and isolated to greater than 95 percent purity with a yield of 1 mg per L of expression media (Figures 1A and S1B). To show CRBN_ΔHBD is a suitable construct for studying binary ligand interactions, affinity differences between purified CRBN:DDB1, CRBN_TBD, and CRBN_ΔHBD were measured against a thalidomide-derived Cy5 tracer molecule in fluorescence polarization (FP) assays¹⁸ (Figure 1B). Similar to previous studies,¹⁶ isolated CRBN_TBD has significantly lower affinity toward the tracer (K_D of 5000 nM \pm 500 nM) when compared with the near full-length CRBN:DDB1 heterodimer (K_D of 4.1 nM \pm 0.8 nM). However, the newly engineered construct, CRBN_ΔHBD, binds the tracer molecule with a K_D of 13 nM \pm 1.6 nM, showing highly similar affinity to CRBN:DDB1. To confirm this behavior across a range of first- and second-generation MGs and PROTACs (Table S1)^{18–23}, competitive FP experiments were performed resulting in highly comparable K_i values (R^2 values of 0.998) between CRBN:DDB1 and CRBN_ΔHBD constructs (Figures 1C–1E). This suggests that CRBN_ΔHBD, like

CRBN:DDB1, is able to adopt a fully functional conformation where engagement of the sensor loop and Lon N domains is required for interaction with high affinity second-generation MGs such as mezigdomide.¹⁵ Stability, and activity of CRBN_ΔHBD was further validated with thermal shift measurements showing monophasic melting curves with mid-point shifts between 6.7 ± 0.3 and $13.8 \pm 0.22^\circ\text{C}$ in the presence of the ligands (Figure S1C), correlating well with measured K_i (Figure S1D).

CRBN_ΔHBD can be used to study ternary PROTAC complex formation

To investigate CRBN_ΔHBD activity in ternary complex formation assays the bromodomain-containing protein 4 (BRD4) PROTAC dBET6¹⁸ was selected (Table S1). Spectral shift assays were optimized to directly calculate the K_D and apparent cooperativity value (α) in the presence of the first bromodomain of purified BRD4 (BRD4-BD1, aa 42–168) (Figure 2A). In line with previously reported literature values dBET6 displays a negative apparent cooperativity of 0.5.¹⁸ For direct visualization of ternary complex formation, size exclusion chromatography-high performance liquid chromatography (SEC-HPLC) elution profiles were recorded for both CRBN_ΔHBD and BRD4-BD1 in presence of dBET6 and additionally CRBN_ΔHBD in the presence of the CRBN homo-PROTAC²³ (Figures S1E and S1F). Both PROTACs yield almost 100 percent ternary complex formation

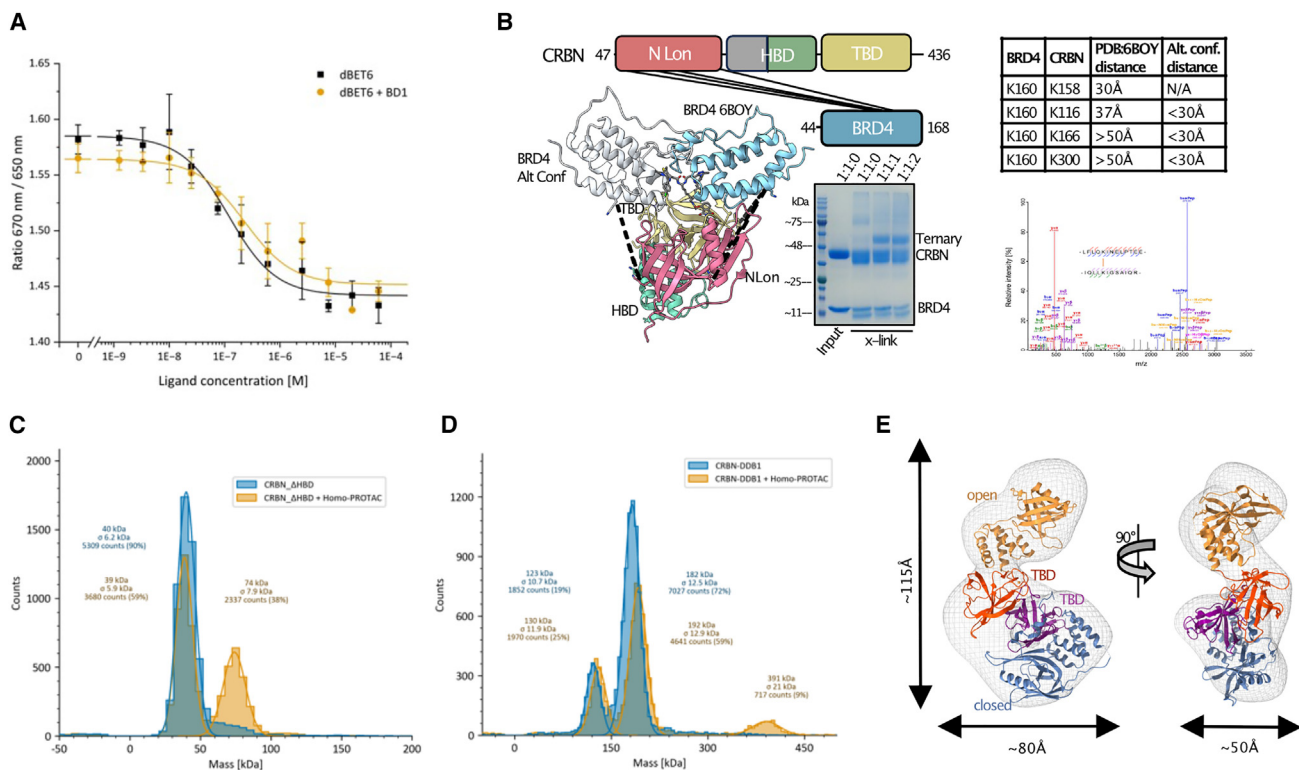


Figure 2. Visualization of complex formation with published tool PROTACs

(A) Spectral shift affinity and cooperativity measurements of binary and ternary complex formation with CRBN_ΔHBD and BRD4-BD1. Data presented as the mean ± SD (n = 4).

(B) SDS-PAGE showing covalent capture of a BRD4:CRBN_ΔHBD ternary complex in the presence of lysine crosslinker and dBET6. Lane 1 contains protein MW marker, lane two contains the input BRD4-BD1 and CRBN_ΔHBD at 1:1 M ratio without DSS crosslinker, lane 3–5 contains 0.2 mM DSS crosslinker with a molar ratio BRD4-BD1:CRBN_ΔHBD:dBET6 of 1:1:0 (lane 3) 1:1:1 (lane 4) and 1:1:2 (lane 5). Crosslinked lysines within the BRD4-CRBN_ΔHBD:dBET6 induced ternary complex identified via LC-MS/MS mapped onto the polypeptide scheme and crystal structure of the BRD4:CRBN:dBET6 complex (PDB: 6BOY).¹⁸ BRD4 is colored blue in the crystal structure and gray in the alternative modeled state. The table shows the distances between C-α atoms of crosslinked lysines in both conformational states. Representative fragmentation spectrum of accepted crosslinks (bottom right) (n = 2).

(C) Refeyn mass photometry measurements of CRBN_ΔHBD showing direct visualization of ternary complex formation after incubation with homo-PROTAC.

(D) Refeyn mass photometry measurements of CRBN:DDB1 complex showing direct visualization of ternary complex formation after incubation with homo-PROTAC.

(E) 3D envelopes calculated from negative stain electron microscopy of CRBN_ΔHBD ternary complex after incubation with homo-PROTAC. CRBN in closed conformation (PDB: 6BOY)¹⁸ and open conformation (PDB: 6BNB)¹⁸ were rigid-body fit into density.

seen through a reduction in retention volume of the individual monomer peaks to single ternary complex elution with increasing PROTAC concentration (Figures S1E and S1F). Ternary complex formation between BRD4-BD1 and CRBN_ΔHBD was further validated in the presence of both dBET6 and the covalent lysine crosslinker disuccinimidyl suberate (DSS, Table S1) using denaturing SDS-PAGE (Figure 2B). Four inter-crosslinked peptides were identified by mass spectrometry (Figure 2B) and mapped onto the crystal structure of CRBN:DDB1ΔB-BRD4_{BD1}-dBET6 (PDB:6BOY)¹⁸ (Figure 2B). When compared against the structure, one of these crosslinks formed with an optimal distance of 30 Å between lysine Cα atoms, indicating the ternary complex with CRBN_ΔHBD is able to adopt a similar conformation to the single state resolved by X-ray crystallography. Three further inter-crosslinks formed with distance restraints greater than the optimal 30 Å, indicating the BRD4-CRBN_ΔHBD ternary complex may sample multiple conformations in solution. Rotation of BRD4-BD1 along a pivot

point within the flexible linker of dBET6 allowed for conformations with appropriate distance restraints for crosslinking (Figure 2B). The dynamic nature of the BRD4:CRBN ternary complexes has been previously reported using hydrogen-deuterium exchange HDX mass spectrometry,²⁴ thus providing further evidence here that single snapshots of ternary complexes via X-ray crystallography are not always representative of the ensemble of solution states.

Oligomeric homogeneity of CRBN_ΔHBD was confirmed by mass photometry (Refeyn) (Figure 2C), where a single homogeneous monomer peak was seen at the expected molecular weight of 40 kDa. Following addition of a CRBN homo-PROTAC, successful ternary complex formation was apparent by appearance of a second peak corresponding to the expected mass of the ternary complex (Figure 2C). Direct comparison of CRBN_ΔHBD and CRBN:DDB1 complex using mass photometry highlights the less favorable, heterogeneous nature of the CRBN:DDB1 complex (Figure 2D). Two peaks were evident in the *apo* sample, one

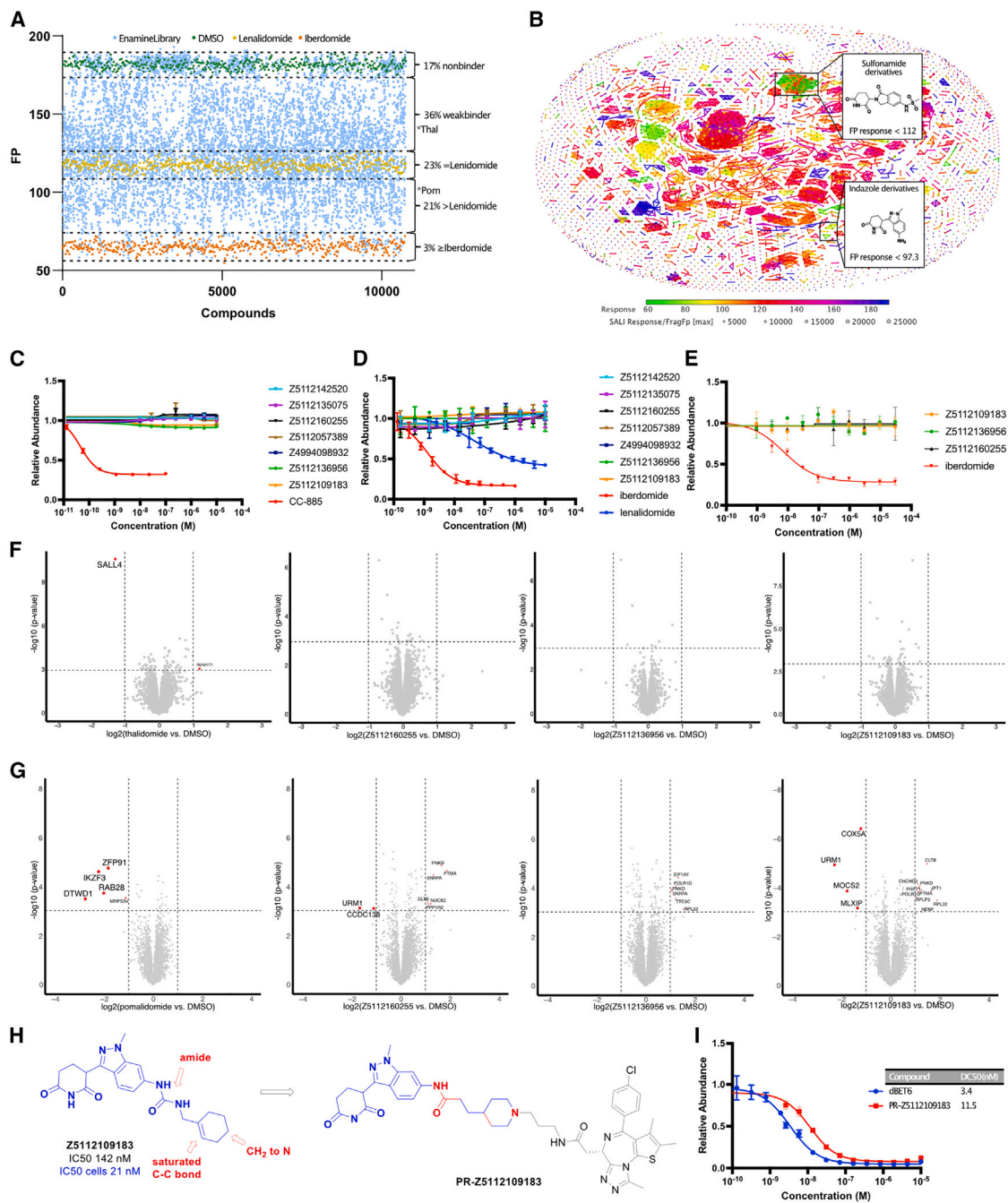


Figure 3. High-throughput screening for discovery of next generation CRBN binders

(A) Single concentration fluorescence polarization competition screen of the focused CRBN library containing 4480 compounds measured in duplicate ($n = 2$). Dashed lines represent 3 times standard deviation of DMSO, lenalidomide and iberdomide controls, ($n = 448$), Z-prime score of 0.85. Asterisk shows response of tool compounds present in the Enamine library.

(B) Structure activity landscape plot of FP response vs. FragFP.

(C) GSPT1 degradation curves for indazole based derivatives. Data are presented as \pm SD ($n = 2$)

(D) Endogenous HiBiT IKZF1 degradation curves for indazole based derivatives in MOLT4 cells. Data are presented as \pm SD ($n = 2$).

(E) Endogenous HiBiT SALL4 degradation curves for indazole based derivatives in SK-N-DZ cells. All curves measured in duplicate. Data are presented as \pm SD ($n = 2$).

(F) Scatterplot displaying relative FC in protein abundance following treatment of Kelly cells for 5h with 1 μ M thalidomide vs. DMSO, Z5112160255 vs. DMSO, Z5112136956 vs. DMSO, Z5112109183 vs. DMSO (left to right) (Data S4) hits are identified via fold-change greater than 2 and $\log_{10} p$ value below 0.001 ($n = 3$).

(legend continued on next page)

corresponding to the expected mass of DDB1 alone at 120 kDa and one corresponding to the CRBN:DDB1 hetero-complex. Addition of CRBN homo-PROTAC to the CRBN:DDB1 complex did not result in any change in the peak at 120 kDa, further indicating this peak corresponds to DDB1 alone (Figure 2D). The significant portion of un-complexed DDB1 is likely caused by the instability and dissociation of the CRBN:DDB1 heterodimer.

CRBN_ΔHBD ternary complex formation in the presence of homo-PROTAC was further interrogated by negative stain electron microscopy. The micrographs revealed highly homogenous monodisperse particles and clear 2-dimensional (2D) classes could be resolved (Figure S1G). Calculation of an electron density map at >15 Å and rigid body fit of both open and closed states of CRBN structures showed that one CRBN molecule is able to adopt an open state conformation with the opposing CRBN molecule adopting the closed state (Figure 2E).

Implementation of CRBN_ΔHBD in high-throughput library screen

Due to its small size and oral availability, thalidomide-based derivatives are highly favorable small molecule E3 handles for the development of PROTACs. Previously, significant issues with off-target toxicity and stability of this chemical scaffold are well-reported.^{25,26} However, recent efforts have led to the exciting discovery of next generation IMiD scaffolds which eliminate undesirable off-target degradation profile.⁸ Having established CRBN_ΔHBD as a relevant construct to study binary and ternary complex formation using tool compounds, we next optimized high-throughput screening assays to search for alternative PROTAC chemical starting points that can also be tested for reduced off-target degradation properties. FP assays were miniaturized to 384-well plates and CRBN_ΔHBD was screened against a CRBN-focused library of 4480 compounds (Enamine). The library was specially designed for the CRBN screening campaigns and investigation of CRBN-based MGs. Thus, 3,650 compounds contain the thalidomide core with various substitutions in the phthaloyl ring as well as the glutarimide ring (Figure S2A), and an additional 830 compounds contained scaffold variation with close similarity to typical IMiD chemotypes (Figure S2B). Synthesis of most of the compounds was performed at Enamine starting from available glutarimide containing building blocks by coupling with diverse counterparts using typical parallel chemistry procedures (Figure S2C). The primary FP screen was performed at a 500 nM compound concentration in duplicates using lenalidomide and iberdomide controls to allow differentiation of FP response between low and high affinity binders (Figure 3A). In total 83% of compounds have detectable binding response against CRBN with a calculated assay Z-prime score of 0.85. 3% of compounds have a binding response equal to iberdomide or greater, 21% of compounds showed a binding response between lenalidomide and iberdomide including the previously well-characterized MG pomalidomide, 23% of compounds had a binding response equal to lenalidomide and 36% compounds display a weaker binding response, including

the well-characterized MG thalidomide (Figures 3A and Data S3). 175 compounds were selected for dose-response measurements and revealed high correlation between calculated half-maximal inhibitory concentration IC₅₀ values and initial response in the primary screen, indicating single shot values are highly applicable for interpretation of structure activity relationships (Figure S3A).

Discovery of next generation IMiDs with minimal off-target degradation

Analysis of the structure activity landscape revealed that the high affinity compounds were predominantly derived from the sub-library of phthaloyl ring derivatives (Figure 3B). However, one indazole based compound (Z4994098932), from the sub-library of IMiD scaffold variations, recently published to have affinity toward CRBN:DDB1 comparable to pomalidomide,²⁷ was also identified in this screen with very similar binding activity (Figures 3B and S3B; Table 1). Our data for this compound confirms the previously reported findings, further validating this compound as a CRBN binder. In addition, 5 previously uncharacterized urea based derivatives at position 6 of the indazole ring were identified in the primary screen and confirmed by dose response (Table 1; Figure S3B) to significantly improve CRBN binding with IC₅₀ values ranging between 122 and 164 nM comparable to the next generation IMiD iberdomide. Several of these next generation indazole based binders are further validated to be highly potent binders in NanoBRET cellular engagement assays with IC₅₀ values in the low nanomolar range (Figure S3E and Table 1). The indazole fragment combines a highly favorable trade-off between high affinity, low molecular weight, and appropriate lipophilicity (clogP) values (Table 1) indicating its potential use in PROTACs which characteristically suffer from high MW (>500 Da) and high lipophilicity values (clogP >5) beyond the classic rule of 5.²⁸ Degradation assays confirmed all indazole-based compounds abrogate degradation of the common CRBN off-targets including GSPT1 (Figures 3C; Table 1) and IKZF1 (Figure S3I) in eGFP fusion, mCherry reporter cells and IKZF1 in endogenous MOLT4 HiBIT reporter cells (Figures 3D; Table 1). The top three potent indazole binders (Z5112109183, Z5112136956, and Z5112160255) were next selected for endogenous HiBIT SALL4 reporter degradation assays in SK-N-DZ cells and further shown to abrogate SALL4 degradation (Figure 3E) suggesting suitability of this scaffold for designing CRBN-based PROTACs with reduced off-target effects. Global proteomics data confirmed this behavior, displaying no off-target degradation of reported CRBN glue substrates compared with first generation IMiD compounds thalidomide in Kelly cells (Figure 3F) and pomalidomide in MOLT-4 cells (Figure 3G). However, two of the indazoles appear to result in some down regulation of URM1 in MOLT-4 cells, a previously undescribed target which lacks canonical CRBN degron motifs (Figure 3G). Interestingly we find that amino substitutions on position 5 and 6 of the indazole ring are tolerated for CRBN binding, yielding it suitable as an exit vector for

(G) As in F but for MOLT-4 cells and pomalidomide vs. DMSO, Z5112160255 vs. DMSO, Z5112136956 vs. DMSO, Z5112109183 vs. DMSO (left to right) (Data S5).

(H) Design of PROTAC molecule PR-Z5112109183 starting from indazole containing hit compound Z5112109183. The *in vitro* IC₅₀ as well as cellular CRBN engagement IC₅₀ is indicated.

(I) Endogenous HiBIT BRD4 degradation curves for PR-Z5112109183 in HEK293T cells. Data are presented as ± SD. All curves measured in duplicate (n = 2).

Table 1. Structure, molecular properties and activity of indazole based CRBN binders

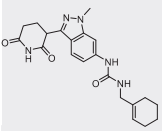
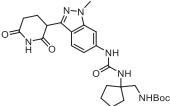
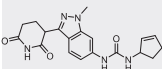
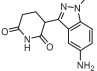
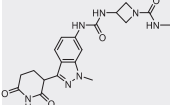
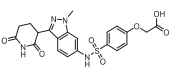
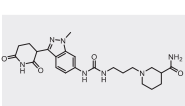
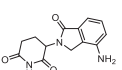
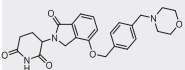
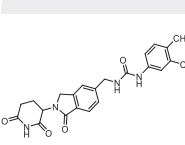
Structure	Enamine ID	MW	clogP	HBAD	TPSA	FP Response	CRBN FP IC ₅₀ [nM]	CRBN cellular engagement IC ₅₀ [nM]	IKZF1 DC ₅₀ [nM]	HiBiT DC ₅₀ [nM]	GSPT1 DC ₅₀ [nM]
	Z5112109183	396	2.13	7	105	69	142	21	No degradation	No degradation	
	Z5112136956	499	2.48	9	143	66	122	26	No degradation	No degradation	
	Z5112160255	367	0.95	7	105	70	158	40	No degradation	No degradation	
	Z4994098932	258	0.45	6	90	97	337	327	No degradation	No degradation	
	Z5112142520	413	0.11	9	137	65	164	443	No degradation	No degradation	
	Z5112057389	473	0.52	11	157	94	278	761	No degradation	No degradation	
	Z5112135075	470	0.07	10	151	69	160	2480	No degradation	No degradation	
	Lenalidomide ^a	259	0.41	6	93	117+-2.9	463	356 +- 210	54.8 +- 15.3		No degradation
	Iberdomide ^a	449	0.53	7	88	65 +-3	150.1	13.4 +- 7.69	1.2 +- 0.08		ND
	CC-885 ^a	441	-	7	108	-	-	-	-		0.05 +- 0.007

Table summarizes molecular properties as well as CRBN FP binding, CRBN NanoBRET target engagement in HEK293T cells, and degradation activity on neosubstrates IKZF1 and GSPT1 as measured in HiBiT and eGFP fusion, mCherry reporter cell lines.

^aIndicates control compounds. HBAD (hydrogen bond donor acceptor), TPSA (topological polar surface area).

PROTAC design (Table 1). To show these indazole based compounds are suitable for development of PROTAC molecules we used the BRD4 inhibitor JQ1, utilized in the dBET PROTAC series,¹⁸ coupled with the best indazole binder, Z5112109183, resulting in PROTAC compound PR-Z5112109183 (Figure 3H). To avoid potential metabolic issues and to simplify the synthesis, we utilized an amide connection instead of a urea motif and replaced the cyclohexene with a 4-substituted piperidine ring, where the piperidine nitrogen served as an exit vector for the linker (Figure 3H). The PROTAC was tested for BRD4 degradation activity in endogenous HiBiT BRD4 reporter cells, revealing

efficient degradation with half-maximal degradation concentration (DC₅₀), after 5 h, in the low nanomolar range (Figure 3I).

In addition to the active binders containing the indazole fragment, several weaker binders with diverse IMiD core variations were identified (Table 2). These include the published compound TD-106 (compound Z3689259904),²⁹ a substituted triazole³⁰ (Z6032284739), and a substituted benzothiazole (Z1694588468) with *in vitro* and cellular binding activity in the nanomolar range (Table 2; Figures S3C and S3F). Their further optimization could be explored for development of potent CRBN-binders with different properties.

Table 2. Structure, molecular properties and activity of diverse glutarimide scaffolds

Structure	Enamine ID	MW	clogP	HBAD	TPSA	FP Response	CRBN FP IC ₅₀ [nM]	CRBN cellular engagement IC ₅₀ [nM]	IKZF1 HiBiT DC ₅₀ [nM]	GSPT1 DC ₅₀ [nM]
	Z6032284739	370	2.38	5	77	118	428	346	No degradation	No degradation
	Z3689259904	273	-0.87	8	117	115	427	358	18.9	No degradation
	Z1694588468	278	1.99	4	59	138	764	659	No degradation	No degradation
	Z4871545631	253	2.25	5	58	141	864	1610	No degradation	No degradation
	Z3076458658	341	1.89	7	84	134	742	2210	No degradation	No degradation
	Z7312613166	442	0.16	9	149	76	189	4490	No degradation	No degradation
	Z4516478784	322	1.38	7	104	136	799	7290	No degradation	No degradation

Table summarizes molecular properties as well as CRBN FP binding, CRBN NanoBRET target engagement in HEK293T cells, and degradation activity on neosubstrates IKZF1 and GSPT1 as measured in HiBiT and eGFP fusion, mCherry reporter cell lines.

We next filtered the screening results based on FP response vs. molecular weight and FP response vs. clogP values and identified several potent scaffolds with IC₅₀ values greater than pomalidomide (Figures S3R and S3S, Data S3) while retaining desirable drug-like properties for potential use as PROTAC warheads. As expected, a number of substitutions in the phthaloyl ring are tolerated or even enhance CRBN binding, while at the same time any close derivatives with even minor changes in the glutarimide part result in low or no activity. Highly enriched among the highest affinity binders in the primary FP screen are a class of compounds with sulfonamide derivatization of carbon 5/6 in the phthaloyl ring (Figures 3B; Table 3). In total 122 sulfonamides exhibited an FP response equivalent to, or better than, lenalidomide, including the simplest sulfonamide derivative Z5000146157 (Table 3 and Data S3). Given the recent identification and prevalence of aryl sulfonamides in DCAF-mediated molecular glues,³¹ it will be highly interesting to explore this family of IMiD-based sulfonamide scaffolds for CRBN-based molecular glue-like functions and to evaluate potential as a PROTAC handle with sulfonamide-containing linkers. The IC₅₀ values of the top 50 hits were confirmed by dose-response measurements to be in the same range as iberdomide and a representative subset of these are displayed (Table 3; Figure S3D). Cellular engagement assays of this subset of 9 sulfonamides revealed 4 derivatives (Z5000145522, Z5000145518, Z5000146291, and Z5000147289) as highly potent, cell permeable CRBN binders. However, likely due to already increased polarity of the sulfonamide group, further incorporation of 2 or more hydrophilic

groups significantly reduced the cellular permeability of this class of compounds. This behavior correlates very well with an increase in the calculated total polar surface area (TPSA) values of the weaker cellular binders (Table 3; Figure S3G). The subset of 9 sulfonamides all abrogate off-target degradation behavior in IKZF1 endogenous HiBiT reporter cells (Table 3; Figure S9N) and IKZF1 in GFP fusion mCherry reporter lines except for the minimal sulfonamide compound (Z5000146157) which had weak degradation activity in IKZF1 GFP fusion mCherry reporter lines only (Figure S9O). In contrast, the sulfonamides displayed variable degradation of GSPT1 in GFP fusion mCherry reporter lines, albeit all significantly reduced compared to control compound CC-885 (Table 3; Figure S9M), as previously published for 2 similar identified CRBN-binding sulfonamide-based compounds.³² Interestingly the top two potent cellular binders (Z5000145522 and Z5000145518) displayed no degradation of IKZF1 and GSPT1. To investigate whether these two compounds can fully abrogate canonical CRBN glue substrate degradation, both compounds were further profiled for degradation activity in endogenous HiBiT SALL4 reporter assays and assessed in global proteomics experiments in MOLT4 and Kelly cells. Surprisingly, despite losing IKZF1 and GSPT1 activity, the sulfonamides showed improved potency for SALL4 degradation, compared with control compound iberdomide, with DC₅₀ values in the picomolar range (Figure S3P). Global proteomics confirmed no IKZF1 degradation activity in both compounds and revealed improved potency for RAB28, believed to be a secondary target of PDE6D,³³ in MOLT4 cells and RAB28 and

Table 3. Structure, molecular properties and activity of sulfonamide based CRBN binders

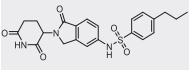
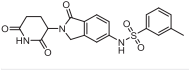
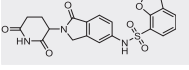
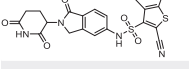
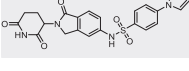
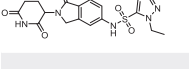
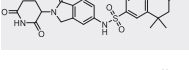
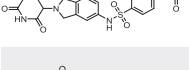
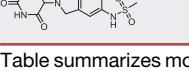
Structure	Enamine ID	MW	clogP	HBAD	TPSA	FP Response	CRBN cellular			
							CRBN FP IC ₅₀ [nM]	engagement IC ₅₀ [nM]	IKZF1 HiBiT DC ₅₀ [nM]	GSPT1 DC ₅₀ [nM]
	Z5000145522	442	2.66	7	113	61	112	18	No degradation	No degradation
	Z5000145518	413	1.60	7	113	62	118	40	No degradation	No degradation
	Z5000146291	439	1.66	7	126	60	118	54	No degradation	Negligible
	Z5000147289	481	2.11	8	136	65	112	241	No degradation	Negligible
	Z5000147880	466	1.07	9	143	65	122	949	No degradation	Negligible
	Z5000147208	417	0.02	8	130	66	107	1390	No degradation	518
	Z5000147527	497	1.61	9	142	64	72	1860	No degradation	483
	Z5000147067	457	0.44	9	142	62	70	2510	No degradation	Negligible
	Z5000146157	337	-0.53	7	113	112	185	3000	No degradation	No degradation

Table summarizes molecular properties as well as CRBN FP binding, CRBN NanoBRET target engagement in HEK293T cells, and degradation activity on neosubstrates IKZF1 and GSPT1 as measured in HiBiT and eGFP fusion, mCherry reporter cell lines.

SALL4 in Kelly cells when compared with first generation IMiD controls (Figure S4). These results confirm sulfonamide modification at carbon 5/6 position in the phthaloyl ring would likely maintain degradation of SALL4 in derived PROTAC molecules. However, this class of 122 sulfonamide based binders will be highly interesting to explore further for changes in potency and specificity among known CRBN substrates.

CRBN_ΔHBD in proof-of-concept cellular molecular glue and PROTAC interactome screening

Finally, having identified diverse CRBN binders with binary binding affinity equivalent to or higher than lenalidomide and unknown molecular glue activity, we next aimed to develop assays which can verify their neosubstrate interactome. To gain insight into IMiD-dependent interactomes of CRBN, we designed a chemo-proteomics approach utilizing recombinantly purified N-terminally FLAG-tagged version of CRBN_ΔHBD for enrichment of ternary complexes in cellular lysates via co-immunoprecipitation (Figure 4A). To show FLAG-CRBN_ΔHBD is active in a cellular screening context MOLT-4 cellular lysates were incubated with immobilized FLAG-CRBN_ΔHBD in the presence and absence of lenalidomide. Analysis of the co-immunoprecipitate via western blot revealed strong enrichment of IKZF1, a validated target of lenalidomide, (Figure S5) as compared to the

DMSO controls. The interactome of FLAG-CRBN_ΔHBD was further analyzed by mass spectrometry in the presence of lenalidomide vs. DMSO (Figure 4B), and pomalidomide vs. DMSO (Figure 4C) confirming IKZF1 enrichment via IMiD mediated interaction with CRBN. Remarkably, in addition to IKZF1, a further six C2H2 zinc finger proteins (Figure 4E) were enriched including known degradation substrates, IKZF3, WIZ1, and RNF166, and previously unreported substrates ZNF521, ZNF217, and IKZF2 (Figure 4E). Beyond the canonical C2H2 zinc finger protein family, 9 additional proteins of diverse structure and function were also enriched as putative CRBN-dependent glue interactors. Structure based sequence alignment, using AlphaFold predicted full length structures,³⁴ confirms five of these hits (ELAVL1, ASS1, SCYL1, MARS1, and ZBED3) contain the minimal surface exposed G-loop degron sequence required to drive complex formation (Figure 4F). In addition to identifying structurally conserved G-loop motifs, AlphaFold3 Multimer³⁵ was able to predict G-loop dependent complex formation between the known substrate IKZF1 and CRBN with an RMSD of 0.8 Å compared with the cryo-EM structure (PDB: 8D80)¹⁵ (Figure 4G). Of the five newly identified G-loop binders, AlphaFold3 Multimer was also able to model canonical G-loop interactions of CRBN with ASS1 and ELAVL1, but not with SCYL1, MARS1, or ZBED3 (Figure 4G). The remaining four proteins identified via

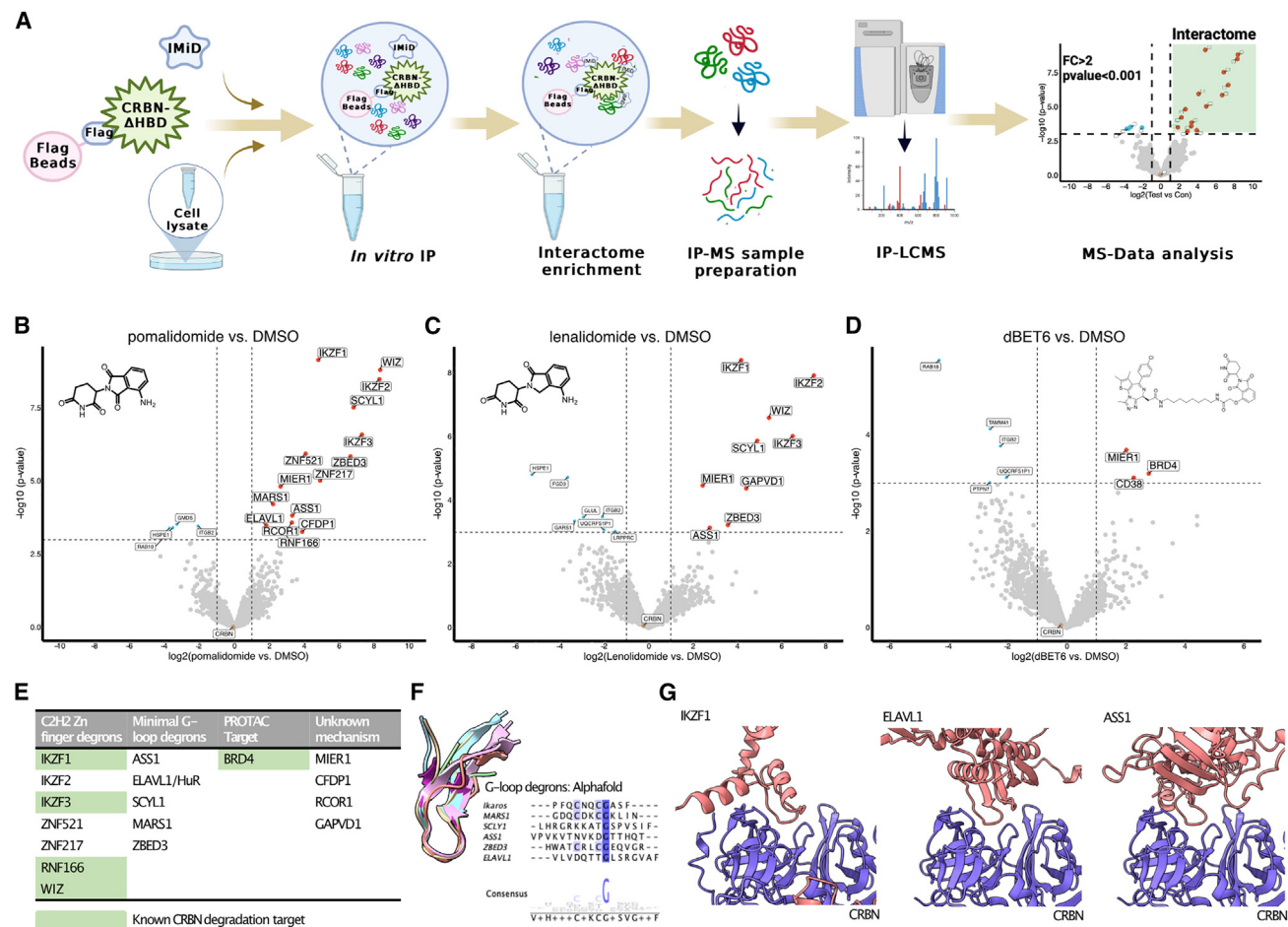


Figure 4. FLAG-tagged CRBN_ΔHBD reveals IMiD interactomes

(A) ProxiCapture target interactomics workflow for determination of IMiD dependent CRBN interactomes via chemoproteomics.

(B) Scatterplot displaying relative FC in protein enrichment after coIP of FLAG-tagged CRBN_ΔHBD with incubation of 5 μM lenalidomide vs. DMSO control in MOLT4 lysates (Data S6) hits are identified via fold-change above 2 and log₁₀ p value below 0.001 (n = 3).

(C) As in C but for pomalidomide (Data S6).

(D) As in C but for dBET6 (Data S6).

(E) Summary table showing all hits across lenalidomide, pomalidomide, and dBET6. Substrates containing minimal exposed G-loops were identified via AlphaFold structure analysis.³⁴

(F) Structure based sequence alignment of identified G-loops in AlphaFold predictions.

(G) AlphaFold3 Multimer³⁵ calculations predicting G-loop mediated ternary complex formation. Left CRBN with IKZF1, middle CRBN with ELAVL1, and right CRBN with ASS1.

chemo-proteomics do not appear to contain the canonical degron sequence required for glue mediated interactions with CRBN and may be recruited via an alternative mechanism or through secondary interactions with degron-containing binders.

To establish whether this screening method can also be a useful tool to investigate interactome specificity of PROTACs during ternary complex formation, the dBET6 interactome was also measured in MOLT-4 cell lysates. dBET6 was specifically chosen due to its negative cooperativity during ternary complex formation (Figure 2A)¹⁸ to test sensitivity of the assay toward lower affinity ternary complexes. The primary degradation target of dBET6, BRD4, was successfully identified as one of three enriched proteins (Figure 4D) highlighting this assay format, in addition to detecting highly cooperative glue complexes, can

also capture PROTAC-mediated ternary complexes with lower affinity.

These results confirm that CRBN_ΔHBD is functional *in vitro* and in cells enabling insights into the interactomes of CRBN-based degraders. The assay provides tools to assess specificity during ternary complex formation and for the identification of potential neosubstrates, which could be exciting candidates for a targeted approach to optimize chemistry for degradation or inhibition of function.

DISCUSSION

In order to resolve the current limitation of CRBN expression for compound screening assays, we developed an intermediate CRBN construct, CRBN_ΔHBD that has been successfully

designed for simple and more efficient protein production in *E. coli* expression systems. CRBN_ΔHBD has equivalent activity to CRBN:DDB1 toward thalidomide-based tool compounds, unlike previous *E. coli*-expressed CRBN constructs. Future use of CRBN_ΔHBD will, therefore, help circumvent the challenges of working with the heterogenous DDB1:CRBN complex in costly insect cell expression systems, providing a more effective construct for validating and ranking degrader compounds based on biophysical properties of binary and ternary complex formation. These data, obtained from the assays optimized here, will be highly desirable for integration with compound cellular target assays and degradation profiles for the rational design and optimization of PROTAC molecules and validation of MGs discovered through phenotypic cellular screening approaches.

The feasibility of the construct in a high-throughput screening approach was further validated by coupling the optimized binding assays with a CRBN-focused IMiD library. The library is specifically designed and regularly updated with IMiD scaffolds by Enamine to search both modified chemical scaffolds that may balance preferable drug like properties with improved ligand affinity and also sample diverse chemical space for potential molecular glue-like functions. Enriched within the highest affinity hits in the library (but not exclusively), we discover both sulfonamide derivatization of carbon in position 5 or 6 in the phthaloyl ring and indazole based derivatives as highly potent classes of CRBN binders *in vitro* and in cells. We further profile the top indazole and sulfonamide-based compounds in CRBN neosubstrate degradation assays and show the indazoles completely abrogate canonical off-target degradation, whereas the top sulfonamides appear to be highly potent and selective SALL4 and RAB28 degraders. Finally we convert the indazole-based CRBN binder to a BRD4-active PROTAC and show it to be a useful alternative compound series for PROTAC warhead design and specificity.

Our binding annotation of the diverse IMiD-based CRBN chemical space will also be highly informative for the exploration of molecular glue-like substrates and modalities. To this end, we successfully developed a FLAG-tagged CRBN construct capable of enriching molecular glues complexes from mammalian cell lysates. Through taking a binding first approach and screening broad interactomes in whole-cell lysates we identify both known C2H2 zinc finger binders and putative minimal G-loop containing binders. The interactome data reported here has the potential to identify both degradation active and inactive molecular glue complexes. Therefore, identification of novel degraders requires combinatorial approaches with target-specific degradation assays. However, we believe this information to be highly valuable, both for specificity analysis of glues and PROTACs and for identification of starting points for targeted degradation screening campaigns or inhibition-of-function modalities. Using published IMiD glues we already show this assay has high potential for discovery of CRBN substrates. Coupling this assay with varied IMiD chemistry, identified in our binary screening efforts, has further potential for identification of additional target classes containing the minimal G-loop degron present in many families of proteins beyond the C2H2 zinc fingers. Furthermore, it is well established both here and previously that small chemical changes can lead to drastic differences in IMiD potency and selectivity toward degron-containing

substrates providing high potential for downstream chemical optimization of novel degradation-active or degradation-inactive functional compounds. Finally, in addition to screening for molecular glues, the IP-MS approach will be highly informative for the profiling of PROTAC specificity and provide additional information on the interactome vs. the degradome of individual PROTACs. Such information will be invaluable for selective targeting of specific isoforms within evolutionary related and structurally similar protein families and help to tune specificity of compounds toward their intended degradation target. We believe that these tools will enable rapid exploration of chemical and neosubstrate space of CRBN and IP-MS methods demonstrated here can extend to other induced proximity systems.

Limitations of the study

There are several important limitations to the assays and resources generated by this study. Firstly, data generated *in vitro* and in cellular lysates using CRBN_ΔHBD provides a simple way to access binding data for both validation and deep exploration of potential binary and ternary complexes; however, it does not provide information on cellular permeability or degradation activity of compounds. Therefore, tools generated here are used in combination with existing methods to explore the different properties of degrader interactions and their potential impact on CRBN substrates. Therefore, chemoproteomics hits require targeted approaches downstream to understand biological outcome of ternary complex formation and to establish whether degradation properties can be optimized. Furthermore, although chemoproteomics assays provide deep insights into specificity of IMiD compounds at a binding level, data are limited by availability of substrates in specific cell lines and amenability of detection via mass spectrometry approaches.

RESOURCE AVAILABILITY

Lead contact

Requests for further information and resources should be directed to and will be fulfilled by Ivan Dikic, dikic@biochem2.uni-frankfurt.de.

Materials availability

Plasmids containing the CRBN_ΔHBD insert generated in this study have been deposited to Addgene. Reagents generated in this study will be made available on request but we may require completed materials transfer agreement if there is potential for commercial application.

Data and code availability

- Data availability: All data reported in this paper will be shared by the [lead contact](#) upon request. Data have been deposited at ProteomeXchange Consortium (<http://proteomecentral.proteomexchange.org>) via the PRIDE partner repository³⁶ and are publicly available as of the date of publication. Accession numbers are listed in the [key resources table](#).
- Code availability: This paper does not report original code.
- Any additional information required to reanalyze the data reported in this paper is available from the [lead contact](#) on request.

ACKNOWLEDGMENTS

We thank all the members of the Dikic laboratory and the members of the PROXIDRUGs consortium for their support and constructive discussion. We thank Se-Hun Kim (Enamine Germany) for the preparation of PR-Z5112109183. We thank all members of the Quantitative Proteomics Unit at IBC2 (Goethe University, Frankfurt), in particular, Martin Adrian-Allgood for

sample preparation and measurements, Kristina Wagner for producing LC columns and David Krause for help in (bio)informatics. We thank the Deutsche Forschungsgemeinschaft (German Research Foundation, DFG) for funding the LC-MS system (easy nLC 1200, QExactive HF) used in this study (project-id: 259130777, SFB1177 – Selective Autophagy). We thank Katherine A. Donovan, Eric S. Fischer and the Fischer Lab Degradation Proteomics Initiative for collection of the global proteomics data supported by NIH CA214608 and CA218278. We thank Sonja Welsch and Susann Kaltwasser from the Central Electron Microscopy facility of the Max Planck Institute of Biophysics for electron microscopy support. Furthermore, we acknowledge Proteros Biostructures GmbH (Munich, Germany) for protein supply of CRBN:DDB1 and BRD4. Finally, we thank members of the SGC Frankfurt screening lab Benedict-Tilman Berger and Lewis Elson for technical screening support. PROXIDRUGS as part of the initiative “Clusters4Future” is funded by the Federal Ministry of Education and Research BMBF (03ZU1109FA). R.P.N. is a member of the excellence cluster ImmunoSensation2 funded by the Deutsche Forschungsgemeinschaft (DFG) under Germany’s Excellence Strategy – EXC2151–390873048. Work by iBET was funded by Fundação para a Ciência e Tecnologia/Ministério da Ciência, Tecnologia e Ensino Superior (FCT/MCTES, Portugal) through national funds to iNOVA4Health (UIDB/04462/2020 and UIDP/04462/2020) and the Associate Laboratory LS4FUTURE (LA/P/0087/2020).

AUTHOR CONTRIBUTIONS

The present study was conceived by I. Dikic, F.J.S., and H.J.B.; J.E. and H.J.B. carried out the majority of structural and biophysical experiments with technical support from E.-M.L. and expertise from A.A.W., F.J.S., and I. Dikic; I.K., T. Matviyuk, and N.T. designed and selected the Enamine library.; H.J.B. carried out primary screening and analysis with expertise from I.K., T. Matviyuk, and N.T.; J.V. carried out crosslinking mass spectrometry experiments with supervision and expertise of J.D.L.; R.K. optimized and performed colP assays and global proteomics assays in Kelly cells with support from V.J.S., G.G., T. Mosler, H.J.B., and I. Dikic; J.G., D.E.P., I. Dressel, and T.M.G. performed IKZF1 and GSPT1 degradation assays and NanoBRET cellular engagement assays with expertise from R.P.N.; U.B. performed SALL4 degradation assays and cell viability assays with expertise from B.L.; A.M.E., S.P.S., R.L.S., and T.M.B performed protein purification and optimization; H.J.B., J.E., F.J.S., R.P.N., I.K., and I. Dressel. wrote the manuscript with contributions from all authors.

DECLARATION OF INTERESTS

Dr Kondratov, Dr Matviyuk, and Dr Tolmachova are current or prior employees of Enamine Ltd.

STAR★METHODS

Detailed methods are provided in the online version of this paper and include the following:

- **KEY RESOURCES TABLE**
- **EXPERIMENTAL MODEL AND STUDY PARTICIPANT DETAILS**
- **METHOD DETAILS**
 - Cloning, expression and purification
 - Fluorescence polarization
 - Thermal stability
 - Spectral shift
 - Mass photometry
 - Analytical SEC
 - X-linking mass spectrometry
 - Negative stain electron microscopy
 - Cellular IKZF1 and GSPT1 degradation assays
 - Cellular BRD4 HiBIT assay
 - Cellular IKZF1 HiBIT assay
 - Cellular SALL4 HiBIT assay
 - Cellular CRBN NanoBRET engagement assay
 - PROTAC synthesis

- Global proteomics in MOLT4 cells
- LC-MS data analysis
- Mass spectrometry sample preparation Kelly cells proteome analysis
- Mass spectrometry data acquisition (proteome)
- Mass spectrometry data analysis (proteome)
- FLAG-CRBN co-immunoprecipitation
- Mass spectrometry sample preparation (co-immunoprecipitation)
- Mass spectrometry data acquisition (co-immunoprecipitation)
- Mass spectrometry data analysis (co-IP)
- CRBN-focused library

● QUANTIFICATION AND STATISTICAL ANALYSIS

SUPPLEMENTAL INFORMATION

Supplemental information can be found online at <https://doi.org/10.1016/j.chembiol.2024.11.002>.

Received: May 15, 2024

Revised: September 24, 2024

Accepted: November 1, 2024

Published: November 27, 2024

REFERENCES

1. Chamberlain, P.P., and Hamann, L.G. (2019). Development of targeted protein degradation therapeutics. *Nat. Chem. Biol.* **15**, 937–944.
2. Burslem, G.M., and Crews, C.M. (2020). Proteolysis-Targeting Chimeras as Therapeutics and Tools for Biological Discovery. *Cell* **181**, 102–114. <https://doi.org/10.1016/j.cell.2019.11.031>.
3. Sakamoto, K.M., Kim, K.B., Kumagai, A., Mercurio, F., Crews, C.M., and Deshaies, R.J. (2001). Protacs: Chimeric molecules that target proteins to the Skp1-Cullin-F box complex for ubiquitination and degradation. *Proc. Natl. Acad. Sci. USA* **98**, 8554–8559. <https://doi.org/10.1073/pnas.141230798>.
4. Winter, G.E., Buckley, D.L., Paulk, J., Roberts, J.M., Souza, A., Dhe-Paganon, S., and Bradner, J.E. (2015). Selective Target Protein Degradation via Phthalimide Conjugation. *Science* **348**, 1376–1381.
5. Mullard, A. (2023). 2022 FDA approvals. *Nat. Rev. Drug Discov.* **22**, 83–88. <https://doi.org/10.1038/d41573-023-00001-3>.
6. Lu, J., Qian, Y., Altieri, M., Dong, H., Wang, J., Raina, K., Hines, J., Winkler, J.D., Crew, A.P., Coleman, K., and Crews, C.M. (2015). Hijacking the E3 Ubiquitin Ligase Cereblon to Efficiently Target BRD4. *Chem. Biol.* **22**, 755–763. <https://doi.org/10.1016/j.chembiol.2015.05.009>.
7. Donovan, K.A., An, J., Nowak, R.P., Yuan, J.C., Fink, E.C., Berry, B.C., Ebert, B.L., and Fischer, E.S. (2018). Thalidomide promotes degradation of SALL4, a transcription factor implicated in Duane radial ray syndrome. *Elife* **7**, e38430. <https://doi.org/10.7554/eLife.38430>.
8. Nguyen, T.M., Srekanth, V., Deb, A., Kokkonda, P., Tiwari, P.K., Donovan, K.A., Shoba, V., Chaudhary, S.K., Mercer, J.A.M., Lai, S., et al. (2024). Proteolysis-targeting chimeras with reduced off-targets. *Nat. Chem.* **16**, 218–228. <https://doi.org/10.1038/s41557-023-01379-8>.
9. Petzold, G., Fischer, E.S., and Thomä, N.H. (2016). Structural basis of lenalidomide-induced CK1 α degradation by the CRL4 CRBN ubiquitin ligase. *Nature* **532**, 127–130. <https://doi.org/10.1038/nature16979>.
10. Matyskiela, M.E., Lu, G., Ito, T., Pagarigan, B., Lu, C.C., Miller, K., Fang, W., Wang, N.Y., Nguyen, D., Houston, J., et al. (2016). A novel cereblon modulator recruits GSPT1 to the CRL4 CRBN ubiquitin ligase. *Nature* **535**, 252–257. <https://doi.org/10.1038/nature18611>.
11. Wang, E.S., Verano, A.L., Nowak, R.P., Yuan, J.C., Donovan, K.A., Eleuteri, N.A., Yue, H., Ngo, K.H., Lizotte, P.H., Gokhale, P.C., et al. (2021). Acute pharmacological degradation of Helios destabilizes regulatory T cells. *Nat. Chem. Biol.* **17**, 711–717. <https://doi.org/10.1038/s41589-021-00802-w>.
12. Chamberlain, P.P., Lopez-Girona, A., Miller, K., Carmel, G., Pagarigan, B., Chie-Leon, B., Rychak, E., Corral, L.G., Ren, Y.J., Wang, M., et al. (2014).

- Structure of the human Cereblon-DDB1-lenalidomide complex reveals basis for responsiveness to thalidomide analogs. *Nat. Struct. Mol. Biol.* 21, 803–809. <https://doi.org/10.1038/nsmb.2874>.
13. Sievers, Q.L., Petzold, G., Bunker, R.D., Renneville, A., Stabicki, M., Liddicoat, B.J., Abdulrahman, W., Mikkelsen, T., Ebert, B.L., and Thomä, N.H. (2018). Defining the human C2H2 zinc finger degrome targeted by thalidomide analogs through CRBN. *Science* 362, eaat0572. <https://doi.org/10.1126/science.aat0572>.
 14. Fischer, E.S., Böhm, K., Lydeard, J.R., Yang, H., Stadler, M.B., Cavadini, S., Nagel, J., Serluca, F., Acker, V., Lingaraju, G.M., et al. (2014). Structure of the DDB1-CRBN E3 ubiquitin ligase in complex with thalidomide. *Nature* 512, 49–53. <https://doi.org/10.1038/nature13527>.
 15. Watson, E.R., Novick, S., Matyskiela, M.E., Chamberlain, P.P., H de la Peña, A., Zhu, J., Tran, E., Griffin, P.R., Wertz, I.E., and Lander, G.C. (2022). Molecular glue CELMoD compounds are regulators of cereblon conformation. *Science* 378, 549–553. <https://doi.org/10.1126/science.aad7574>.
 16. Mori, T., Ito, T., Liu, S., Ando, H., Sakamoto, S., Yamaguchi, Y., Tokunaga, E., Shibata, N., Handa, H., and Hakoshima, T. (2018). Structural basis of thalidomide enantiomer binding to cereblon. *Sci. Rep.* 8, 1294. <https://doi.org/10.1038/s41598-018-19202-7>.
 17. Boichenko, I., Bär, K., Deiss, S., Heim, C., Albrecht, R., Lupas, A.N., Hernandez Alvarez, B., and Hartmann, M.D. (2018). Chemical Ligand Space of Cereblon. *ACS Omega* 3, 11163–11171. <https://doi.org/10.1021/acsomega.8b00959>.
 18. Nowak, R.P., Deangelo, S.L., Buckley, D., He, Z., Donovan, K.A., An, J., Safaee, N., Jedrychowski, M.P., Ponthier, C.M., Ishoey, M., et al. (2018). Plasticity in binding confers selectivity in ligand-induced protein degradation article. *Nat. Chem. Biol.* 14, 706–714. <https://doi.org/10.1038/s41589-018-0055-y>.
 19. Zhao, M., Hu, M., Chen, Y., Liu, H., Chen, Y., Liu, B., and Fang, B. (2021). Cereblon modulator CC-885 induces CRBN-dependent ubiquitination and degradation of CDK4 in multiple myeloma. *Biochem. Biophys. Res. Commun.* 549, 150–156. <https://doi.org/10.1016/j.bbrc.2021.02.110>.
 20. Carrancio, S., Grocock, L., Janardhanan, P., Jankeel, D., Galasso, R., Guarinos, C., Narla, R.K., Groza, M., Leisten, J., Pierce, D.W., et al. (2021). CC-99282 is a Novel Cereblon (CRBN) E3 Ligase Modulator (CELMoD) Agent with Enhanced Tumoricidal Activity in Preclinical Models of Lymphoma. *Blood* 138, 1200. <https://doi.org/10.1182/blood-2021-148068>.
 21. Matyskiela, M.E., Zhang, W., Man, H.W., Muller, G., Khambatta, G., Baculi, F., Hickman, M., Lebrun, L., Pagarigan, B., Carmel, G., et al. (2018). A Cereblon Modulator (CC-220) with Improved Degradation of Ikaros and Aiolos. *J. Med. Chem.* 61, 535–542. <https://doi.org/10.1021/acs.jmedchem.6b01921>.
 22. Hansen, J.D., Correa, M., Nagy, M.A., Alexander, M., Plantevin, V., Grant, V., Whitefield, B., Huang, D., Kercher, T., Harris, R., et al. (2020). Discovery of CRBN E3 Ligase Modulator CC-92480 for the Treatment of Relapsed and Refractory Multiple Myeloma. *J. Med. Chem.* 63, 6648–6676. <https://doi.org/10.1021/acs.jmedchem.9b01928>.
 23. Steinebach, C., Lindner, S., Udeshi, N.D., Mani, D.C., Kehm, H., Köpf, S., Carr, S.A., Gütschow, M., and Krönke, J. (2018). Homo-PROTACs for the Chemical Knockdown of Cereblon. *ACS Chem. Biol.* 13, 2771–2782. <https://doi.org/10.1021/acscchembio.8b00693>.
 24. Eron, S.J., Huang, H., Agafonov, R.V., Fitzgerald, M.E., Patel, J., Michael, R.E., Lee, T.D., Hart, A.A., Shaulsky, J., Nasveschuk, C.G., et al. (2021). Structural Characterization of Degradation-Induced Ternary Complexes Using Hydrogen-Deuterium Exchange Mass Spectrometry and Computational Modeling: Implications for Structure-Based Design. *ACS Chem. Biol.* 16, 2228–2243. <https://doi.org/10.1021/acscchembio.1c00376>.
 25. SCHUMACHER, H., SMITH, R.L., and WILLIAMS, R.T. (1965). THE METABOLISM OF THALIDOMIDE: THE FATE OF THALIDOMIDE AND SOME OF ITS HYDROLYSIS PRODUCTS IN VARIOUS SPECIES. *Br. J. Pharmacol. Chemother.* 25, 338–351. <https://doi.org/10.1111/j.1476-5381.1965.tb02054.x>.
 26. Kim, J.H., and Scialli, A.R. (2011). Thalidomide: The tragedy of birth defects and the effective treatment of disease. *Toxicol. Sci.* 122, 1–6. <https://doi.org/10.1093/toxsci/kfr088>.
 27. Norris, S., Ba, X., Rhodes, J., Huang, D., Khambatta, G., Buenviaje, J., Nayak, S., Meiring, J., Reiss, S., Xu, S., et al. (2023). Design and Synthesis of Novel Cereblon Binders for Use in Targeted Protein Degradation. *J. Med. Chem.* 66, 16388–16409. <https://doi.org/10.1021/acs.jmedchem.3c01848>.
 28. Edmondson, S.D., Yang, B., and Fallan, C. (2019). Proteolysis targeting chimeras (PROTACs) in 'beyond rule-of-five' chemical space: Recent progress and future challenges. *Bioorg. Med. Chem. Lett.* 29, 1555–1564. <https://doi.org/10.1016/j.bmcl.2019.04.030>.
 29. Kim, S.A., Go, A., Jo, S.H., Park, S.J., Jeon, Y.U., Kim, J.E., Lee, H.K., Park, C.H., Lee, C.O., Park, S.G., et al. (2019). A novel cereblon modulator for targeted protein degradation. *Eur. J. Med. Chem.* 166, 65–74. <https://doi.org/10.1016/j.ejmech.2019.01.023>.
 30. Ronnebaum, J.M., and Luzzio, F.A. (2016). Synthesis of 1,2,3-triazole 'click' analogues of thalidomide. *Tetrahedron* 72, 6136–6141. <https://doi.org/10.1016/j.tet.2016.07.019>.
 31. Hsia, O., Hinterdorfer, M., Cowan, A.D., Iso, K., Ishida, T., Sundaramoorthy, R., Nakasone, M.A., Imrichova, H., Schätz, C., Rukavina, A., et al. (2023). Targeted protein degradation via intramolecular bivalent glues. *Nature* 627, 204–211. <https://doi.org/10.1101/2023.02.14.528511>.
 32. Nishiguchi, G., Keramatnia, F., Min, J., Chang, Y., Jonchere, B., Das, S., Actis, M., Price, J., Chepyala, D., Young, B., et al. (2021). Identification of Potent, Selective, and Orally Bioavailable Small-Molecule GSPT1/2 Degradation from a Focused Library of Cereblon Modulators. *J. Med. Chem.* 64, 7296–7311. <https://doi.org/10.1021/acs.jmedchem.0c01313>.
 33. Teng, M., Lu, W., Donovan, K.A., Sun, J., Krupnick, N.M., Nowak, R.P., Li, Y.D., Spering, A.S., Zhang, T., Ebert, B.L., et al. (2022). Development of PDE6D and CK1 α Degradation through Chemical Derivatization of FFFT-2216. *J. Med. Chem.* 65, 747–756. <https://doi.org/10.1021/acs.jmedchem.1c01832>.
 34. Varadi, M., Bertoni, D., Magana, P., Paramval, U., Pidruchna, I., Radhakrishnan, M., Tsenkov, M., Nair, S., Mirdita, M., Yeo, J., et al. (2024). AlphaFold Protein Structure Database in 2024: providing structure coverage for over 214 million protein sequences. *Nucleic Acids Res.* 52, D368–D375. <https://doi.org/10.1093/nar/gkad1011>.
 35. Abramson, J., Adler, J., Dunger, J., Evans, R., Green, T., Pritzel, A., Ronneberger, O., Willmore, L., Ballard, A.J., Bambrick, J., et al. (2024). Accurate structure prediction of biomolecular interactions with AlphaFold 3. *Nature* 630, 493–500. <https://doi.org/10.1038/s41586-024-07487-w>.
 36. Perez-Riverol, Y., Bai, J., Bandla, C., García-Seisdedos, D., Hewapathirana, S., Kamatchinathan, S., Kundu, D.J., Prakash, A., Frericks-Zipper, A., Eisenacher, M., et al. (2022). The PRIDE database resources in 2022: A hub for mass spectrometry-based proteomics evidences. *Nucleic Acids Res.* 50, D543–D552. <https://doi.org/10.1093/nar/gkab1038>.
 37. Furihata, H., Yamanaka, S., Honda, T., Miyauchi, Y., Asano, A., Shibata, N., Tanokura, M., Sawasaki, T., and Miyakawa, T. (2020). Structural bases of IMiD selectivity that emerges by 5-hydroxythalidomide. *Nat. Commun.* 11, 4578. <https://doi.org/10.1038/s41467-020-18488-4>.
 38. Krieger, J., Sorrell, F.J., Wegener, A.A., Leuthner, B., Machrouhi-Porcher, F., Hecht, M., Leibrock, E.M., Müller, J.E., Eisert, J., Hartung, I.V., and Schlesiger, S. (2023). Systematic Potency and Property Assessment of VHL Ligands and Implications on PROTAC Design. *ChemMedChem* 18, e202200615. <https://doi.org/10.1002/cmdc.202200615>.
 39. Nowak, R.P., Che, J., Ferrao, S., Kong, N.R., Liu, H., Zerfas, B.L., and Jones, L.H. (2023). Structural rationalization of GSPT1 and IKZF1 degradation by thalidomide molecular glue derivatives. *RSC Med. Chem.* 14, 501–506. <https://doi.org/10.1039/d2md000347c>.
 40. Zerfas, B.L., Huerta, F., Liu, H., Du, G., Gray, N.S., Jones, L.H., and Nowak, R.P. (2023). Advancing targeted protein degrader discovery by

- measuring cereblon engagement in cells. *Methods Enzymol.* **681**, 169–188. <https://doi.org/10.1016/bs.mie.2022.08.013>.
41. Meier, F., Brunner, A.D., Frank, M., Ha, A., Bludau, I., Voytik, E., Kaspar-Schoenefeld, S., Lubeck, M., Raether, O., Bache, N., et al. (2020). diaPASEF: parallel accumulation–serial fragmentation combined with data-independent acquisition. *Nat. Methods* **17**, 1229–1236. <https://doi.org/10.1038/s41592-020-00998-0>.
 42. Demichev, V., Messner, C.B., Vernardis, S.I., Lilley, K.S., and Ralser, M. (2020). DIA-NN: neural networks and interference correction enable deep proteome coverage in high throughput. *Nat. Methods* **17**, 41–44. <https://doi.org/10.1038/s41592-019-0638-x>.
 43. McAlister, G.C., Nusinow, D.P., Jedrychowski, M.P., Wühr, M., Huttlin, E.L., Erickson, B.K., Rad, R., Haas, W., and Gygi, S.P. (2014). MultiNotch MS3 enables accurate, sensitive, and multiplexed detection of differential expression across cancer cell line proteomes. *Anal. Chem.* **86**, 7150–7158.
 44. Kong, A.T., Leprevost, F.V., Avtonomov, D.M., Mellacheruvu, D., and Nesvizhskii, A.I. (2017). MSFragger: Ultrafast and comprehensive peptide identification in mass spectrometry-based proteomics. *Nat. Methods* **14**, 513–520. <https://doi.org/10.1038/nmeth.4256>.
 45. da Veiga Leprevost, F., Haynes, S.E., Avtonomov, D.M., Chang, H.Y., Shanmugam, A.K., Mellacheruvu, D., Kong, A.T., and Nesvizhskii, A.I. (2020). Philosopher: a versatile toolkit for shotgun proteomics data analysis. *Nat. Methods* **17**, 869–870. <https://doi.org/10.1038/s41592-020-0912-y>.
 46. Yu, F., Haynes, S.E., and Nesvizhskii, A.I. (2021). IonQuant enables accurate and sensitive label-free quantification with FDR-controlled match-between-runs. *Mol. Cell. Proteomics* **20**, 100077. <https://doi.org/10.1016/J.MCPRO.2021.100077>.
 47. Hsiao, Y., Zhang, H., Li, G.X., Deng, Y., Yu, F., Valipour Kahrood, H., Steele, J.R., Schittenhelm, R.B., and Nesvizhskii, A.I. (2024). Analysis and Visualization of Quantitative Proteomics Data Using FragPipe-Analyst. *J. Proteome Res.* **23**, 4303–4315. <https://doi.org/10.1021/acs.jproteome.4c00294>.

STAR★METHODS

KEY RESOURCES TABLE

REAGENT or RESOURCE	SOURCE	IDENTIFIER
Bacterial and virus strains		
<i>E. coli</i> BL21 (DE3) Tuner cells	Sigma Aldrich	Cat#70623
Chemicals, peptides, and recombinant proteins		
Human CRBN:DDB1 complex (CRBN (40–442) and DDB1(1–1140))	Proteros Biostructures GmbH	N/A
CRBN_ΔHBD (residues 47 to 193 and 249 to 436)	This study	N/A
CRBN-TBD (amino acids 318–426)	This study	N/A
Human BRD4-BD1(42–168)	This study	N/A
Enamine IMiD Library	Enamine LTD	Cat#IMiD-4900
Thalidomide	Merck Healthcare KGaA	N/A
Lenalidomide	Merck Healthcare KGaA	N/A
Pomalidomide	Merck Healthcare KGaA	N/A
Iberdomide	Merck Healthcare KGaA	N/A
Mezigdomide	Merck Healthcare KGaA	N/A
CC-885	Merck Healthcare KGaA	N/A
DBET6	Merck Healthcare KGaA	N/A
HomoPROTAC	Merck Healthcare KGaA	N/A
CRBN FP tracer	bio-technie TOCRIS	Cat#7288
BODIPY TM -lenalidomide fluorescent tracer	WuXi Apptec	N/A
PR-Z5112109183	This study	N/A
Critical commercial assays		
NanoBRET® Target Engagement Intracellular Assays	Promega®	Cat#N2160
Nano-Glo® HiBiT Lytic Detection System	Promega®	Cat#N3030
CellTiter-Glo® Luminescent Cell Viability Assay	Promega®	Cat#G7570
Deposited data		
ProteomeXchange Consortium: Global Proteomics in Kelly cells and Co-IP data	This study	PXD056863; https://proteomecentral.proteomexchange.org/ui
ProteomeXchange Consortium: Global Proteomics in MOLT4 cells	This study	PXD057393; https://proteomecentral.proteomexchange.org/ui
ProteomeXchange Consortium: Cross linking mass spectrometry data of CRBN:DBET6:BRD4	This study	PXD048871; https://proteomecentral.proteomexchange.org/ui
Crystal structure of DDB1-CRBN-BRD4(BD1) complex bound to dBET6 PROTAC	RCSB Protein dataBank	PDB 6BOY; https://www.rcsb.org/structure/6BOY
Cereblon ~ DDB1 bound to Iberdomide and Ikaros ZF1-2-3	RCSB Protein dataBank	PDB 8D80; https://www.rcsb.org/structure/8D80
Crystal structure of DDB1-CRBN-BRD4(BD1) complex bound to dBET57 PROTAC	RCSB Protein dataBank	PDB 6BNB; https://www.rcsb.org/structure/6BNB
Experimental models: Cell lines		
Flp293T cells	Center for Protein Degradation, Dana-Farber Cancer Institute, Boston, MA, 02215, USA	N/A
HiBiT-BRD4 HEK293T cells	Fischer Lab, Dana-Farber Cancer Institute	N/A
HiBiT-IKZF1 MOLT4 cells	Fischer Lab, Dana-Farber Cancer Institute	N/A

(Continued on next page)

Continued

REAGENT or RESOURCE	SOURCE	IDENTIFIER
HiBiT-SALL4- KI SK-N-DZ cells	Promega®	N/A
HEK293T/17 cells	ATCC	Cat#CRL-11268
Kelly cells	Dana-Farber Cancer Institute	N/A
MOLT4 cells	Winter Lab, GEMM	N/A
Oligonucleotides		
Forward primer to clone CRBN_ΔHBD 'GTAATGGAACTCTGGTGATGCTG AGACCTTAATGGACAGA'	IDT	N/A
Reverse primer to clone CRBN_ΔHBD 'CAGAGTTTCCATTACCGTTGAAGG CAACACACATTCG'	IDT	N/A
Mutagenesis forward primer to clone flag CRBN_ΔHBD 'ACAAGGATGACGACGAT AAGCACCACCATCATCACTCT'	IDT	N/A
Mutagenesis reverse primer to clone flag CRBN_ΔHBD 'ACAAGGATGACGACGAT AAGCACCACCATCATCACTCT'	IDT	N/A
Recombinant DNA		
PLASMID: pnic-MBP, nt MBP-His ₆ tagged CRBN (amino acids 47 to 193 and 249 to 436)	This study	N/A
Virus: CRBN (amino acids 40–442)	Proteros Biostructures GmbH	N/A
Virus: DDB1(amino acids 1–1140) ct Strep tag	Proteros Biostructures GmbH	N/A
Plasmid: pET28a, Human CRBN TBD, His-GB1-3C-Cxxx 318-426	This study	N/A
Plasmid: nt His ₆ tagged BRD4-BD1 (amino acids 42–168)	This study	N/A

EXPERIMENTAL MODEL AND STUDY PARTICIPANT DETAILS

Kelly (donor sex: female) and MOLT4 (donor sex: male) cells were maintained in RPMI (Gibco, Life Technologies) supplemented with 10% fetal bovine serum (FBS) (Gibco, Life Technologies) and 1% penicillin/streptomycin (Gibco, Life Technologies). HEK293T, Flp293T (donor sex: female). in DMEM (Gibco, Life Technologies) supplemented with 10% FBS (Gibco, Life Technologies) KI SK-N-DZ (donor sex female) cells were maintained DMEM medium (DMEM compl, 1xNEAA (Invitrogen 31885023, 11140), 10mM HEPES, 0.5% Penicillin/Streptomycin, 10% FBS).

METHOD DETAILS

Cloning, expression and purification

Human CRBN-TBD (amino acids 318–426) was expressed and purified from *E. coli* as previously described.³⁷ Human BRD4-BD1(42–168) was expressed and purified as previously described.³⁸ Human CRBN:DDB1 complex (CRBN(40–442) and DDB1(1–1140)) was provided by Proteros Biostructures GmbH. For preparation of CRBN_ΔHBD, DNA insert containing CRBN_ΔHBD was cloned into pnic-MBP vectors, Recombinant expression of MBP-His₆ and MBP-FLAG-His₆ CRBN (residues 47 to 193 and 249 to 436) (Data S1) was carried out in *E. coli* BL21 (DE3) Tuner cells grown in Terrific Broth Auto Induction Medium supplemented with 50 μg/mL kanamycin at 37°C. When optical density at 600 nm reached 1.8, cultures were supplemented with 50 μM ZnCl₂ and temperature decreased to 18°C. Over-expression of CRBN proceeded overnight. After harvesting by centrifugation, cells were resuspended in 50 mM HEPES pH 7.5, 500 mM NaCl, 10% glycerol, 2 mM MgCl₂, 0.5 mM Tris(2-carboxyethyl)phosphine hydrochloride (TCEP), 0.02 U/μL GENIUS nuclease (Santa Cruz Biotechnology, Inc.) and cOmplete Protease Inhibitor Cocktail (Roche) and disrupted using a continuous flow Z Basic Cell disruptor (Constant Systems) at 15000 Psi and 4°C. Cell debris were removed by centrifugation at 25862g for 1h30 min at 4°C and supernatant recovered for protein purification. After filtration with a Sartolab P20 filter (Sartorius), supernatant was loaded into a HisTrap Excel column (Cytiva) equilibrated with 50 mM HEPES pH 7.5, 500 mM NaCl, 10% glycerol and 0.5 mM TCEP and unspecific proteins removed by washing the column with the same buffer. CRBN binding to the resin was eluted by increasing concentration of imidazole up to 300 mM. Fractions containing CRBN were selected, loaded into a dialysis membrane, and left overnight at 4°C in dialysis buffer to remove imidazole (50 mM HEPES pH 7.5, 500 mM NaCl, 10% glycerol and 0.5 mM TCEP). Immediately before injection into a Hitrap Q HP column (Cytiva), NaCl concentration

was decreased from 500 mM to 80 mM. CRBN was eluted from the column with 210 mM NaCl and incubated overnight at 4°C with TEV protease for His-tag removal. After incubation and validation of tag cleavage by SDS-PAGE and anti-His western blot, sample was injected into a Superdex 75 26/60 equilibrated with 50 mM HEPES pH 7.5, 200 mM NaCl, 10% glycerol and 0.5 mM TCEP. A main peak corresponding to untagged CRBN monomer was isolated. As a last polishing step, concentration of NaCl was decreased to 50 mM and CRBN was injected into a Hitrap Q HP column (Cytiva). Pure CRBN_ΔHBD was eluted with ~180 mM NaCl and concentrated to 9 mg/mL.

Fluorescence polarization

Cy5-conjugated thalidomide (20 nM) was mixed with increasing concentration of either CRBN:DDB1, CRBN_ΔHBD or CRBN_TBD in 384-well microplates (Greiner) and incubated for 15 min at RT (50 mM HEPES pH 7.5, 200 mM NaCl, 0.5 mM TCEP, 5% glycerol 0.01% Tween). The change in fluorescence polarization was monitored using a PHERAstar FS microplate reader (BMG Labtech). The Cy5-conjugated thalidomide bound fraction was calculated and the K_i was obtained from 2 technical and 2 biological duplicates. Compounds in Cy5-conjugated thalidomide displacement assay were dispensed in a 384-well microplate (Greiner) Echo-Dispenser normalized to 0.6% DMSO. Cy5-conjugated thalidomide (20 nM) and concentration of CRBN:DDB1, CRBN_ΔHBD or CRBN_TBD at 65% saturation in the K_D curves in 25 mM HEPES pH 7.5, 200 mM NaCl, 0.01% TWEEN. were performed. The change in fluorescence polarization across compound titrations was monitored using a PHERAstar FS microplate reader (BMG Labtech). Data from three independent replicates ($n = 3$) were plotted and K_i values obtained. CRBN_ΔHBD was screened using the same set up against a CRBN-focused library of 4480 compounds in duplicate at 500 nM concentration. Hit thresholds were selected 3 time beyond the standard deviation of DMSO control. Compound titration for calculation of IC_{50} of 175 hits were performed in duplicate.

Thermal stability

NanoDSF measurements were performed using Prometheus NT.Plex from NanoTemper. CRBN_ΔHBD at a final concentration of 0.3 mg/mL (50 mM HEPES pH 7.5, 200 mM NaCl, 0.5 mM TCEP, 5% glycerol, 1% DMSO) was measured for stability changes in presence and absence of 50 μM ligands. The temperature was increased from room temperature to 95°C, with a ramp of 1°C per minute and stability monitored by changes in 330 fluorescence. All binding and control measurements were done in biological duplicates.

Spectral shift

Spectral shift measurements were performed using the Monolith X (NanoTemper). CRBN protein was labeled with RED-Maleimide 2nd Generation dye (NanoTemper) optimized for degree-of-labeling of 1:1 M ratio calculated by nanodrop. An 11-point PROTAC dilution series from 60 μM to 1.25 nM, normalized to 0.6% DMSO plus one DMSO control, were dispensed into 10 μL of Labeled CRBN_ΔHBD 10 mM concentration (20 mM HEPES, 200 mM NaCl, 1 mM TCEP, 0.01% Tween 20, 5% Glycerol, pH 7.5) in the presence and absence of purified BRD4 at a fixed concentration of 5 μM. The samples were loaded to Monolith Premium Capillaries (NanoTemper), after 5 min centrifugation of the plate at 3,000 × g at 25°C. The measurements were performed with medium IR power and auto-excitation power at 25°C and fluorescence was detected and plotted for ratio metric changes in 650 and 670 nm wavelengths. Data plotting, K_D calculation was carried out using MO.Control software (NanoTemper). All measurements were performed in 2 technical and 2 biological duplicates.

Mass photometry

Mass photometry measurements were performed using a Two MP Auto (Refeyn). Zeiss high-precision microscope cover glasses 24 × 50 mm with CultureWell reusable gaskets (50 - 3 mm, DIA × 1 mm depth, 3–10 μL) were transferred to the laser lens covered with a drop of Immersol 518 F from Zeiss. 16 μL of mass photometry buffer (20 mM HEPES, 150 mM NaCl, pH 7.5) followed by 4 μL of 100 nM protein solution was transferred to a gasket well. To reach the final assay concentration 20 nM. The ratiometric contrast was evaluated using MP Discovery software in a 1 min movie and converted to mass values, using a standard curve of marker proteins of known mass.

Analytical SEC

Analytical SEC was carried out using a 1260 Infinity II high-pressure liquid chromatography (HPLC) system from Agilent Technologies (Santa Clara, USA), with an AdvanceBio SEC 300 A 2.7 μm column. The final assay concentration of the proteins was set to 12.5 μM in a total volume of 35 μL (20 mM HEPES, 200 mM NaCl, 1 mM TCEP, 0.01% Tween 20, 5% Glycerol, pH 7.5). Ligands and DMSO controls were pre-incubated for 10 min at RT followed by centrifugation for 15 min at 22,000 × g. The samples were transferred to a 96-well plate and stored at 15°C in the HPLC autosampler. The proteins were detected at a wavelength of 280 nm and complex formation was determined according to retention time and integral of the peaks.

X-linking mass spectrometry

Proteins at 15 μM were preincubated for 15 min at RT in presence and absence of dBET6 PROTAC at 1:1 or 1:2 M ratio (50 mM HEPES pH 7.5, 200 mM NaCl, 0.5 mM TCEP, 5% glycerol). Disuccinimidyl suberate crosslinker (ThermoFischer) was spiked 3 times over 30 min to final conc of 0.25 mM and crosslinking reaction was quenched by addition of 150 mM ammonium bicarbonate. The gel band corresponding to the crosslinked complex was excised and digested with trypsin. Excised gel bands were digested using the

In-Gel Tryptic Digestion Kit (Thermo Fisher Scientific, Dreieich, Germany). The gel pieces were destained, reduced and alkylated according to the manufacturers protocol. Digestion was performed overnight at 30°C in a 25:1 ratio of protein:trypsin (SERVA, Heidelberg, Germany). Digested peptides were transferred into a clean tube with 5 µL 0.1% formic acid (FA) in H₂O. Further peptides were extracted from the gel pieces using 10 µL of 1% FA in H₂O and added to the digestion mixture. Peptides were injected onto an Acclaim PepMap C18 capillary trapping column (particle size 3 µm, L = 20 mm) and separated on a ReproSil C18-PepSep analytical column (particle size = 1.9 µm, ID = 75 µm, L = 15 cm, Bruker Cooperation, Billerica, USA) using a nano-HPLC (Dionex U3000 RSLCnano) at a temperature of 55°C. Trapping was performed at a flow rate of 6 µL/min for 6 min using a loading buffer composed of 0.05% trifluoroacetic acid in H₂O. Peptide separation was carried out at a constant flow rate of 400 nL/min using a gradient of water (buffer A: 100% H₂O and 0.1% FA) and acetonitrile (buffer B: 80% ACN, 20% H₂O, and 0.1% FA). The gradient increases from 4% to 48% buffer B in 30 min. All solvents were LC-MS grade and purchased from Riedel-de Hën/Honeywell (Seelze, Germany). Eluting peptides were analyzed in data-dependent acquisition mode on an Orbitrap Eclipse mass spectrometer (Thermo Fisher Scientific, Dreieich, Germany) that is connected to the nano-HPLC by a Nano Flex ESI source. MS1 full scans were acquired over a range of 380–1400 mass-to-charge ratio (m/z) in the Orbitrap detector (resolution = 60k, automatic gain control (AGC) = 4e6, and maximum injection time: 50 ms). Sequence information was acquired by a “ddMS2 OT HCD” MS2 method with a fixed cycle time of 2 s for MS/MS scans. MS2 scans were generated from the most abundant precursors with a minimum intensity of 5e4 and charge states from 3 to 8. Selected precursors were isolated in the quadrupole using a 1.6 Da window and fragmented using higher-energy collisional dissociation (HCD) at 25.3% normalized collision energy. For Orbitrap MS2, an AGC of 1e5 and a maximum injection time of 70 ms were used (resolution = 30k). Dynamic exclusion was set to 60 s with a mass tolerance of 10 parts per million (ppm). The sample was measured in technical duplicates. MS raw data were processed using the MaxQuant software (v2.3.0.0) with customized parameters for the Andromeda search engine. Spectra were matched to a FASTA file containing the sequences of human CRBN and BRD4 (UniProtKB, March 2023) and a decoy and contaminant database. In addition, a list of *E. coli* proteins that were identified with ≥ 5 unique peptides in the sample on a previous search against the *E. coli* proteome (UniProt Proteomes, March 2023) was added. The minimum tryptic peptide length was set to 7 with a maximum of two missed cleavage sites. Carboxyamidomethylation of cysteine residues (static modification), methionine oxidation and acetylation of the protein N-terminus were included (variable modifications) in the search parameters. Precursor mass tolerance was set to 4.5 ppm and fragment ion tolerance to 20 ppm. A false discovery rate (FDR) below 1% was applied for the identification of crosslinks, peptides, and modifications. Crosslinked peptides were manually inspected and evaluated for consistent identification in both technical replicates. The mass spectrometry crosslinking data have been deposited to the ProteomeXchange Consortium (<http://proteomecentral.proteomexchange.org>) via the PRIDE partner repository³⁶ with the dataset identifier PXD048871.

Negative stain electron microscopy

CRBN_ΔHBD at 0.15 mg/mL (150 mM NaCl, 25 mM HEPES pH 7.5, 0.5 mM TCEP) was pre-incubated with Homo-PROTAC at 1:2 M ratio (1% DMSO). The samples were diluted 10-fold immediately prior to grid staining Carbon coated grids (C flat™, 300 Mesh) from were glow discharged. 3 µL of the protein sample was transferred to the grid and incubated for 30 s negatively stained with 2% (w/v) uranyl formate and analyzed by negative-stain electron microscopy with a Rio16 CMOS camera (Gatan) on a Tecnai Spirit (FEI Company) transmission electron microscope (TEM) operated at 120 kV.

Cellular IKZF1 and GSPT1 degradation assays

IKZF1Δ and GSPT1 constructs for the cellular degradation assays were generated as previously described.^{11,18} Flp293T cells were seeded at 75% confluency in 96 well plates (655 180, Cellstar) a day before compound treatment. Compound dose responses were prepared in 96 well plates (655 180, Cellstar) with an Echo Acoustic Dispenser (Labcyte) and frozen until use. To prepare the compound incubation, the cell plate media was exchanged with 50 µL of the compounds, resuspended in 100 µL of DMEM (41966052, LifeTech), supplemented with 10% FBS. The compounds were incubated with cells in duplicate dose responses for 5h following trypsinization and resuspension in FCAS buffer (PBS, 2% FBS, 1 mM EDTA), transferred into U- or V-bottom 96-well plates (650101, 651101, Greiner) and analyzed by flow cytometer (guava easyCyte HT Luminex, Millipore). Signals from a minimum of 3000 events per well were acquired and the eGFP and mCherry fluorescence measured. Data analysis was assisted by using FlowJo (FlowJo, LCC). Live cells with enriched mCherry were determined via forward/side scatter and eGFP/mCherry signal. To quantify the eGFP protein abundance relative to mCherry, a 10-fold amplified ratio for each individual cell was calculated using the formula: 10*eGFP/mCherry. The median of the ratio was then calculated per set and normalized against the DMSO control. The data were plotted in GraphPad Prism 10 and the curves were fitted using Variable Slope equation to obtain the DC₅₀ values.

Cellular BRD4 HiBiT assay

HEK293T cells with N-terminal HiBiT knock in at the BRD4 locus (gift from Fischer Lab). HiBiT-BRD4 HEK293T cells were seeded at 10,000 cells per well in a 384-well plate (Corning, 3570) at 50 µL per well in DMEM media (Thermo Fisher Scientific, 41966-029) containing 10% FBS and compounds were dispensed using D300e Digital Dispenser (Tecan) and normalized to 0.51% DMSO. Cells were incubated at 37°C, 5% CO₂ with the compounds for 5h in duplicate dose responses. HiBiT assay was performed as described in the manufacturer protocol (Promega, N3030). Briefly, 12.5 µL of premixed detection reagent was added to each well of the 384 well

assay plate using ClipTip Pipettes (Thermo Fisher) and incubated for 15 min. The luminescence signal was quantified using PHERAstar FSX microplate reader (BMG Labtech). Data were analyzed using GraphPad Prism 10 software with curve fitting performed using Variable Slope equation.

Cellular IKZF1 HiBiT assay

To run the assay, compounds were first dispensed in dose dilution into 384-well white flat bottom TC-treated plates (Corning, 3570) using Echo Acoustic Dispenser (Labcyte). On the day of the assay, compound plate was thawed and HiBiT-IKZF1 MOLTA³⁹ cells were seeded at 10,000 cells per well in 50 μ L of RPMI (Thermo Fisher Scientific, 21875-034) media and incubated for 5h at 37°C, 5% CO₂. HiBiT assay was performed as described in the manufacturer protocol (Promega, N3030). 12.5 μ L of premixed detection reagent was added to each well of the 384 well assay plate using ClipTip Pipettes (Thermo Fisher) and incubated for 15 min. The luminescence signal was quantified using PHERAstar FSX microplate reader (BMG Labtech). Duplicate dose response data were analyzed using GraphPad Prism 10 software with curve fitting performed using Variable Slope equation.

Cellular SALL4 HiBiT assay

15 μ L of 3000 HiBiT-SALL4- KI SK-N-DZ cells (Promega, Madison, USA) were seeded in complemented DMEM medium (DMEM compl, 1xNEAA (Invitrogen 31885023, 11140), 10mM HEPES, 0.5% Penicillin/Streptomycin, 10% FBS) in 384 well white cell culture microtiter plates (781080, Greiner, Germany) and incubated for 24 h at 37°C and 5% CO₂. Compound serial dilutions were prepared starting with highest concentration of 10 mM resp 0.3 mM with 3x dilution factor in 100% DMSO in 10 concentration points. 45 nL of compound solution resp DMSO were added to the wells by a Labcyte Echo (Beckman Coulter, USA) to generate dose responses in duplicate and plates were incubated for 24 h at 37°C and 5% CO₂. Plates were cooled to room temperature and 15 μ L HiBiT lytic detection reagent (Promega, Madison, USA) according to the manufacturer's instruction were added. Plates were incubated for 20 min by gentle shaking and luminescence was measured with a Pherastar multimode reader (BMG Labtech, Germany). As positive control media only was used, as negative control 100% DMSO was used for normalization. Iberdomide was applied as reference control in a dose-response curve. Normalization and calculation of DC₅₀ and D_{max} was performed with Genedata Analyzer (Gene data, Switzerland). In parallel with the same assay set-up a CellTiter-Glo assay (Promega) was performed to monitor viability effects caused by the compounds.

Cellular CRBN NanoBRET engagement assay

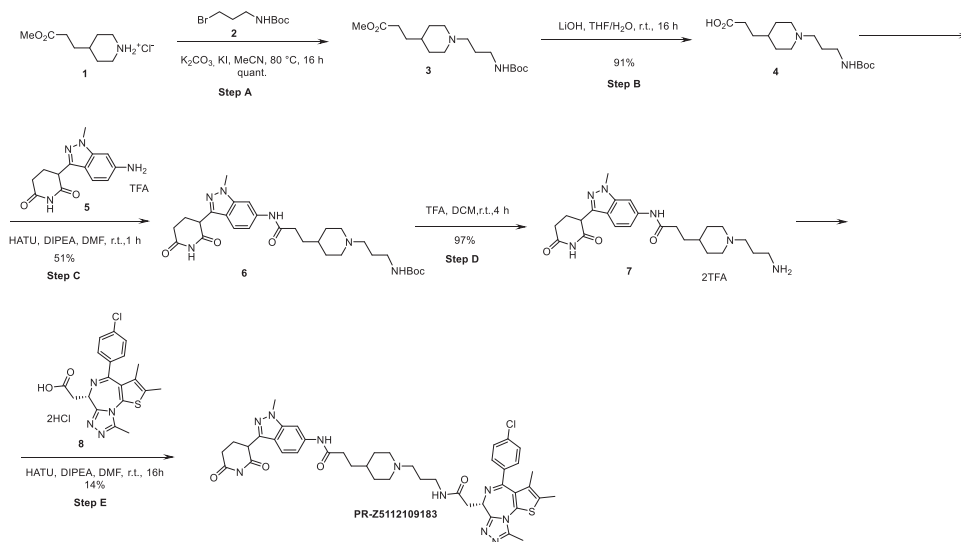
The assay was performed as previously described.⁴⁰ HEK293T stably expressing NanoLuc-CRBN were cultured in DMEM (Gibco, Life Technologies) supplemented with 10% FBS. Cells were resuspended at 2×10^5 viable cells/mL in 21 mL Opti-MEM I (Gibco, Life Technologies) and mixed with 600 μ L BODIPY-lenalidomide fluorescent tracer (stock at 10 μ M diluted in tracer dilution buffer 31.25% PEG-400, 12.5 mM HEPES, pH 7.5, filtered using a 0.22 μ m nitrocellulose membrane) to reach final concentration of the tracer at 278 nM. The cell-tracer mixture was then plated in a white polystyrene 384-well plate (Corning, 3570) at 50 μ L/well. After plating, the assay plate was centrifuged (400 \times g, 5 min) and protected from light. Compounds for testing were added to the plate using a D300e Digital Dispenser (Tecan) in duplicate 12-pt titrations from a 10 mM stock in DMSO, with DMSO normalized to 1% total volume. The plate was then placed in an incubator at 37°C, 5% CO₂ for 2 h. After incubation, the plate was removed and set on the bench to cool to room temperature (~10 min). The NanoLuc substrate (500 \times solution, Promega Catalog number N2160 for 1,000 assay kit) and extracellular inhibitor (1500 \times solution, Promega Catalog number N2160 for 1,000 assay kit) were diluted in Opti-MEM I (Gibco, Life Technologies) to prepare a 3 \times solution, which was added to each well (25 μ L/well). The plate was read on a Pherastar FSX (BMG Labtech) microplate reader with simultaneous dual emission capabilities to read 384-well plates at 450 and 520 nm, for 10 cycles which were averaged to create data points. The NanoBRET ratio was calculated by dividing the signal at 520 nm by the signal at 450 nm and multiplying by 1000 for each sample. The data were plotted in GraphPad Prism 10 and the curves were fitted using Variable Slope equation to obtain the IC₅₀ values.

PROTAC synthesis

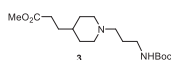
Starting reagents were used as purchased from Enamine Ltd. The products were purified by automated flash chromatography using Biotage Selekt or Interchim PuriFlash XS520 chromatography systems and prepacked Biotage Sfär, Interchim PuriFlash or Büchi FlashPure Select columns. Preparative HPLC was performed on an Agilent 1290 Infinity II Preparative LC System equipped with an Agilent 6120 Quadrupole LC/MS mass detector using Chromatorex SMB C18 (100 \times 19 mm, 5 μ m) and XBridge BEH C18 (100 \times 20 mm, 5 μ m) columns. Analytical LC/MS was performed on Agilent 1260 Infinity and Agilent 1260 Infinity II systems equipped with an Agilent 6120 Quadrupole LC/MS mass detector and an Agilent 380-ELSD detector using Avantor ACE UltraCore 2.5 SuperC18 (50 \times 4.6 mm, 2.5 μ m), Agilent Poroshell 120 SB C18 (30 \times 4.6 mm, 2.7 μ m) and Interchim US5C18HQ-050/046 (50 \times 4.6 mm, 5 μ m) columns. Analytical TLC was performed on pre-coated silica gel plates (Macherey-Nagel, Polygram SIL G/UV254). Visualization was accomplished with UV light, KMnO₄ solution, cerium(IV)/ammonium molybdate solution or ninhydrin solution. ¹H, ¹³C and ¹⁹F NMR spectra were recorded with a Bruker Avance Neo 400 [400 MHz (¹H), 100 MHz (¹³C), 377 MHz (¹⁹F)] spectrometer. Chemical shifts are reported in ppm (δ) with respect to TMS, and the not fully deuterated solvent peak was used for referencing.

2-((S)-4-(4-Chlorophenyl)-2,3,9-trimethyl-6H-thieno[3,2-f][1,2,4]triazolo[4,3-a][1,4]diazepin-6-yl)-N-(7-(3-(N-(2-(2,6-dioxopiperidin-3-yl)-1-oxoisindolin-5-yl)sulfamoyl)phenyl)heptyl)acetamide (PR-Z5112109183).

Synthesis was carried out following the scheme given below:

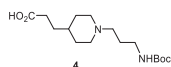


Step A: Methyl 3-(1-(3-((*tert*-Butoxycarbonyl)amino)propyl)piperidin-4-yl)propanoate (**3**)



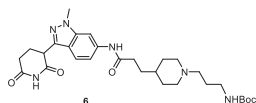
To a solution of methyl 3-(piperidin-4-yl)propanoate hydrochloride **1** (500 mg, 2.41 mmol, 1 eq.) in MeCN (10 mL) was added *tert*-butyl N-(3-bromopropyl)carbamate **2** (688 mg, 2.89 mmol, 1.2 eq.), K_2CO_3 (1.33 g, 9.63 mmol, 4 eq.), KI (480 mg, 2.89 mmol, 1.2 eq.) and stirred at 80 °C for 16 h. The reaction mixture was diluted with ethyl acetate (20 mL) and washed with water (20 mL), brine (20 mL), dried over Na_2SO_4 and concentrated *in vacuo*. Compound **3** (790 mg, 2.41 mmol, quant.) was obtained as a yellow oil which was used without further purification. LC/MS (CI) $m/z = 329.0$ $[M + H]^+$. LC/MS purity >95%.

Step B: 3-(1-(3-((*tert*-Butoxycarbonyl)amino)propyl)piperidin-4-yl)propanoic acid (**4**)



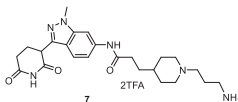
To a solution of compound **3** (790 mg, 2.41 mmol, 1 eq.) in THF (20 mL) was added lithium hydroxide (175 mg, 7.31 mmol, 3 eq.) in water (2 mL) and stirred at room temperature for 16 h. The reaction mixture was concentrated *in vacuo* and the residue was taken up in DCM (50 mL) and acidified to pH 3 with 1 M HCl solution. The aqueous phase was extracted with DCM (2 × 20 mL) and the combined organic phase was washed with brine (2 × 10 mL), dried over Na_2SO_4 and concentrated *in vacuo*. Compound **4** (700 mg, 2.22 mmol, 91%) was obtained as a yellow solid, which was used without further purification. LC/MS (CI) $m/z = 315.0$ $[M + H]^+$, LC/MS purity >95%.

Step C: *tert*-Butyl (3-(4-(3-(3-(2,6-Dioxopiperidin-3-yl)-1-methyl-1H-indazol-6-yl)amino)-3-oxopropyl)piperidin-1-yl)propyl)carbamate (**6**)



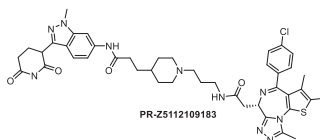
To a solution of compound **4** (338 mg, 1.07 mmol, 2 eq.) in DMF (10 mL) was added HATU (409 mg, 1.07 mmol, 2 eq.), DIPEA (0.37 mL, 2.15 mmol, 4 eq.) and 3-(6-amino-1-methyl-1H-indazol-3-yl)piperidine-2,6-dione trifluoroacetate **5** (200 mg, 0.54 mmol, 1 eq.) and stirred at room temperature for 1 h. The reaction mixture was quenched with water (10 mL) and extracted with ethyl acetate (2 × 20 mL). The combined organic phase was washed with brine (2 × 20 mL), dried over Na_2SO_4 and concentrated *in vacuo*. The residue was purified by FC(C18, $H_2O/MeOH$, 0 → 50%) to afford compound **6** (151 mg, 0.27 mmol, 51%) as a yellow solid. LC/MS (CI) $m/z = 555.0$ $[M + H]^+$, LC/MS purity >95%.

Step D: 3-(1-(3-Aminopropyl)piperidin-4-yl)-N-(3-(2,6-dioxopiperidin-3-yl)-1-methyl-1H-indazol-6-yl)propanamide ditrifluoroacetate (**7**)



To a solution of compound **6** (151 mg, 0.27 mmol, 1 eq.) in DCM (4 mL) was added trifluoroacetic acid (1 mL) and stirred at room temperature for 4 h. The reaction mixture was concentrated in vacuo to yield compound **7** (180 mg, 0.26 mmol, 97%) as colorless oil (ditrifluoroacetate salt). LC/MS (CI) $m/z = 455.0$ $[M + H]^+$, LC/MS purity >95%.

Step E: 2-((S)-4-(4-Chlorophenyl)-2,3,9-trimethyl-6H-thieno[3,2-f][1,2,4]triazolo[4,3-a][1,4]diazepin-6-yl)-N-(7-(3-(N-(2-(2,6-dioxopiperidin-3-yl)-1-oxoisindolin-5-yl)sulfamoyl)phenyl)heptyl)acetamide (**PR-Z5112109183**)



To a solution of JQ-1 dihydrochloride **8** (104 mg, 0.22 mmol, 1.5 eq.) in DMF (4 mL) was added HATU (84 mg, 0.22 mmol, 1.5 eq.), DIPEA (0.13 mL, 0.73 mmol, 5 eq.) and compound **7** (100 mg, 0.15 mmol, 1 eq.) and stirred at room temperature for 16 h. The reaction mixture was quenched with water (5 mL) and extracted with ethyl acetate (2 × 10 mL). The combined organic phase was washed with brine (2 × 10 mL), dried over Na_2SO_4 and concentrated in vacuo. The residue was purified by FC(C18, $\text{H}_2\text{O}/\text{MeOH}$, 0 → 50%) to afford the title compound PR-Z5112109183 (17 mg, 0.02 mmol, 14%) as a white solid. LC/MS (CI) $m/z = 836.8$ $[M + H]^+$, LC/MS purity >95%. ^1H NMR (400 MHz, $\text{DMSO}-d_6$) δ 10.88 (s, 1H), 10.11 (s, 1H), 8.39 (s, 1H), 8.07 (s, 1H), 7.61 (d, $J = 8.8$ Hz, 1H), 7.48 (d, $J = 8.8$ Hz, 2H), 7.44 (d, $J = 8.7$ Hz, 2H), 7.10 (d, $J = 9.7$ Hz, 1H), 4.52 (t, $J = 7.3$ Hz, 1H), 4.30 (dd, $J = 9.7, 5.1$ Hz, 1H), 3.91 (s, 3H), 3.45 (m, 1H), 3.29–3.20 (m, 3H), 3.14–3.06 (m, 3H), 3.03–2.78 (m, 3H), 2.67–2.62 (m, 2H), 2.59 (s, 3H), 2.41 (s, 3H), 2.39–2.29 (m, 3H), 2.21–2.15 (m, 1H), 1.94–1.84 (m, 2H), 1.81–1.75 (m, 2H), 1.63 (s, 3H), 1.61–1.53 (m, 3H), 1.53–1.39 (s, 1H), 1.37–1.23 (m, 2H) (Data S2).

Global proteomics in MOLT4 cells

MOLT4 cells were treated with DMSO, or 1 μM compounds in biological triplicates for 6 h. Cells were lysed by addition of lysis buffer (8 M Urea, 50 mM NaCl, 50 mM 4-(2-hydroxyethyl)-1-piperazineethanesulfonic acid (EPPS) pH 8.5, Protease and Phosphatase inhibitors) and homogenization by bead beating (BioSpec) for three repeats of 30 s at 2400 strokes/min. Bradford assay was used to determine the final protein concentration in the clarified cell lysate. Fifty micrograms of protein for each sample were reduced, alkylated and precipitated using methanol/chloroform as previously described⁷ and the resulting washed precipitated protein was allowed to air dry. Precipitated protein was resuspended in 4 M urea, 50 mM HEPES pH 7.4, followed by dilution to 1 M urea with the addition of 200 mM EPPS, pH 8. Proteins were digested with the addition of LysC (1:50; enzyme:protein) and trypsin (1:50; enzyme:protein) for 12 h at 37°C. Sample digests were acidified with formic acid to a pH of 2–3 before desalting using C18 solid phase extraction plates (SOLA, Thermo Fisher Scientific). Desalted peptides were dried in a vacuum-centrifuged and reconstituted in 0.1% formic acid for liquid chromatography-mass spectrometry analysis.

Data were collected using a TimSTOF Pro2 (Bruker Daltonics, Bremen, Germany) coupled to a nanoElute LC pump (Bruker Daltonics, Bremen, Germany) via a CaptiveSpray nano-electrospray source. Peptides were separated on a reversed-phase C_{18} column (25 cm × 75 μm ID, 1.6 μm , IonOpticks, Australia) containing an integrated captive spray emitter. Peptides were separated using a 50 min gradient of 2–30% buffer B (acetonitrile in 0.1% formic acid) with a flow rate of 250 nL/min and column temperature maintained at 50°C.

Data-dependent acquisition (DDA) was performed in parallel accumulation-serial fragmentation (PASEF) mode to determine effective ion mobility windows for downstream diaPASEF data collection.⁴¹ The ddaPASEF parameters included: 100% duty cycle using accumulation and ramp times of 50 ms each, 1 TIMS-MS scan and 10 PASEF ramps per acquisition cycle. The TIMS-MS survey scan was acquired between 100 and 1700 m/z and $1/k_0$ of 0.7–1.3 V s/cm^2 . Precursors with 1–5 charges were selected and those that reached an intensity threshold of 20,000 arbitrary units were actively excluded for 0.4 min. The quadrupole isolation width was set to 2 m/z for $m/z < 700$ and 3 m/z for $m/z > 800$, with the m/z between 700 and 800 m/z being interpolated linearly. The TIMS elution voltages were calibrated linearly with three points (Agilent ESI-L Tuning Mix Ions; 622, 922, 1,222 m/z) to determine the reduced ion mobility coefficients ($1/K_0$). To perform diaPASEF, the precursor distribution in the DDA m/z -ion mobility plane was used to design an acquisition scheme for Data-independent acquisition (DIA) data collection which included two windows in each 50 ms diaPASEF scan. Data were acquired using sixteen of these 25 Da precursor double window scans (creating 32 windows) which covered the diagonal scan line for doubly and triply charged precursors, with singly charged precursors able to be excluded by their position in the m/z -ion mobility plane. These precursor isolation windows were defined between 400 and 1200 m/z and $1/k_0$ of 0.7–1.3 V s/cm^2 .

LC-MS data analysis

The diaPASEF raw file processing and controlling peptide and protein level false discovery rates, assembling proteins from peptides, and protein quantification from peptides were performed using library free analysis in DIA-NN 1.8.⁴² Library free mode performs an in silico digestion of a given protein sequence database alongside deep learning-based predictions to extract the DIA precursor data into a collection of MS2 spectra. The search results are then used to generate a spectral library which is then employed for the targeted analysis of the DIA data searched against a Swissprot human database (January 2021). Database search criteria largely followed the default settings for directDIA including: tryptic with two missed cleavages, carbamidomethylation of cysteine, and oxidation of methionine and precursor Q-value (FDR) cut-off of 0.01. Precursor quantification strategy was set to Robust LC (high accuracy) with RT-dependent cross run normalization. Proteins with low sum of abundance (<2,000 x no. of treatments) were excluded from further analysis and proteins with missing values were imputed by random selection from a Gaussian distribution either with a mean of the non-missing values for that treatment group or with a mean equal to the median of the background (in cases when all values for a treatment group are missing). Protein abundances were scaled using in-house scripts in the R framework (R Development Core Team, 2014) and resulting data were filtered to only include proteins that had a minimum of 3 counts in at least 4 replicates of each independent comparison of treatment sample to the DMSO control. Significant changes comparing the relative protein abundance of these treatment to DMSO control comparisons were assessed by moderated t test as implemented in the limma package within the R framework (M.E. Ritchie et al., 2015, *Nucleic Acids Res*, 43(7):e47).

Mass spectrometry sample preparation Kelly cells proteome analysis

Kelly cells were treated with DMSO, or 1 μ M compounds in biological triplicates ($N = 3$) for 5h. Cells were harvested and washed with PBS by centrifugation. Further, Lysis buffer (2% SDS, 50mM Tris pH 8.5, 10mM TCEP, 40mM CAA, supplemented with protease inhibitor cocktail) was added to the pellets and cells were homogenized by sonication in ice and boiling at 95°C for 10 min. Proteins were precipitated using methanol-chloroform and resuspended in 8 M urea, 50 mM Tris pH 8.5. Bradford assay was used to determine final protein concentration in the lysate. 50 μ g of proteins were digested with 1:50 w/w LysC (Wako Chemicals, cleaves at the carboxylic side of lysine residue) and 1:100 w/w trypsin (Promega, Sequencing-grade) overnight at 37°C after dilution to a final urea concentration of 1 M using 50 mM Tris pH 8.5. Digested peptides were then acidified (pH 2–3) using trifluoroacetic acid (TFA) and purified using C18 SepPak columns (Waters). Desalted peptides were dried and resuspended in TMT-labeling buffer (200 mM EPPS pH 8.2, 20% acetonitrile). 10 μ g of peptides per condition were subjected to TMT labeling with 1:2.5 peptide TMT ratio (w/w) for 1 h at room temperature. The labeling reaction was quenched by addition of hydroxylamine to a final concentration of 0.5% and incubation at room temperature for 15 min. Successful TMT labeling was verified by mixing equimolar ratios of peptides and subjecting the mix to single shot LC-MS/MS analysis. For high pH reversed phase fractionation on a Dionex analytical HPLC, 50 μ g of pooled and purified TMT labeled samples were resuspended in 10mM ammonium-bicarbonate (ABC), 5%ACN, and separated on a 250mm long C18 column (Aeris Peptide XB-C18, 4.6mm ID, 2.6 μ m particle size; Phenomenex) using a multistep gradient from 100% Solvent A (5% ACN, 10mM ABC in water) to 60% Solvent B (90% ACN, 10mM ABC in water) over 70 min. Eluting peptides were collected every 45 s into a total of 96 fractions, which were cross-concatenated into 24 fractions and dried in a vacuum concentrator and resuspended in 3% ACN, 0.1% TFA for LC-MS analysis.

Mass spectrometry data acquisition (proteome)

Tryptic peptides were analyzed on Orbitrap Ascend coupled to a VanquishNeo (ThermoFisher Scientific) using a 25 cm long, 75 μ m ID fused-silica column packed in house with 1.9 μ m C18 particles (Reprosil pur, Dr. Maisch), and kept at 50°C using an integrated column oven (Sonation). HPLC solvents consisted of 0.1% Formic acid in water (Buffer A) and 0.1% Formic acid, 80% Acetonitrile in water (Buffer B). Assuming equal amounts in each fraction, 250 ng of peptides were eluted by a non-linear gradient from 7 to 40% B over 90 min, followed by a stepwise increase to 90%B in 6 min which was held for another 9 min. A synchronous precursor selection (SPS) multi-notch MS3 method was used to minimize ratio compression as previously described (McAlister et al⁴³). Full-scan MS spectra (350–1400 m/z) were acquired at a resolution of 120,000 at m/z 200, a maximum injection time of 100 ms, and an AGC target value of 4×10^5 . The most intense precursors with charge state between 2 and 6 were selected for fragmentation (“Top Speed” with a cycle time of 1.5 s) and isolated with a quadrupole isolation window of 0.7 Th. MS2 scans were performed in the Ion trap (Turbo) using a maximum injection time of 35ms, AGC target value of 30000 and fragmented using CID with a normalized collision energy (NCE) of 35%. SPS-MS3 scans for quantification were triggered only after successful Real-time search against the mouse canonical reference proteome from SwissProt with the same search parameter as stated below for data processing in Proteome Discoverer. Criteria for passing the search were Xcorr: 1, dCn: 0.1 and precursor mass accuracy: 10 ppm. Maximum search time was 35ms. MS3 acquisition was performed on the 10 most intense MS2 fragment ions with an isolation window of 0.7 Th (MS) and 2 m/z (MS2). Ions were fragmented using HCD with an NCE of 50% and analyzed in the Orbitrap with a resolution of 45,000 at m/z 200, scan range of 100–200 m/z, AGC target value of 150000 and a maximum injection time of 91ms. Repeated sequencing of already acquired precursors was limited by setting a dynamic exclusion of 60 s and 7 ppm and advanced peak determination was deactivated. All spectra were acquired in centroid mode.

Mass spectrometry data analysis (proteome)

MS raw data were analyzed using FragPipe v21.1, with MSFragger v.4.0⁴⁴ and Philosopher v.5.1.0.⁴⁵ The built-in workflows “TMT10-MS3” and “TMT16-MS3” were used with a precursor mass tolerance of 20 ppm and fragment mass tolerance of 20 ppm. The human proteome database used by FP (ID: UP000005640, 09/03/2024) comprised of 20,468 reviewed sequences only and their corresponding decoys, including common contaminant proteins. Identifications were filtered to obtain false discovery rates (FDR) below 1% for both peptide spectrum matches (minimum peptide length of 7) and proteins using a target-decoy strategy. For all searches, carbamidomethylated cysteine was set as a fixed modification and oxidation of methionine and N-terminal protein acetylation as variable modifications with allowing up to 3 modifications per peptide. Strict trypsin cleavage was set as protein digestion rule. Label-free quantification was performed using IonQuant v.1.10.27.⁴⁶ Data were further processed using FragPipe Analyst.⁴⁷ Subsequently, the data were plotted in R using custom scripts.

FLAG-CRBN co-immunoprecipitation

Purified FLAG-CRBN was conjugated to FLAG beads (cat no ffak, Chromotek) in IP buffer (50mM Tris pH-7.5, 120mM NaCl, 1% NP40, 0.5mM EDTA) for 1 h at 4°C on a rotating shaker, before addition of DMSO or 5μM Lenalidomide/Pomalidomide/dBET6 for 30 min at 4°C. Subsequently, ~1mg of freshly prepared protein lysate from Molt4 cells was added to the prepared beads in IP lysate buffer (50mM Tris pH-7.5, 120mM NaCl, 1% NP40, 0.5mM EDTA, protease inhibitors, phosphatase inhibitors and NEM) for 1 h at 4°C while rotating in biological triplicates ($N = 3$). The beads were washed three times with IP buffer and afterward used either for western blotting or trypsin digestion followed by LC-MS² analysis.

Mass spectrometry sample preparation (co-immunoprecipitation)

Protein-bound FLAG-CRBN beads were incubated with 20 μL SDC buffer (3% sodium deoxycholate in 50 mM Tris-HCl pH 8.5) and heated for 5 min at 65°C and supernatant was collected. This step was repeated one more time to get elute of 40μL. Further, reduction and alkylation were performed using 5 ul of 5mM TCEP, 20mM CAA in 50 mM Tris-HCl pH 8.5 at 95°C for 10min 500 ng of trypsin in 45 μL 50 mM Tris-HCl (pH 8.5) was added to each sample and kept it for digestion at 37 °C overnight. The digestion was stopped upon addition of 150 μL of 1% TFA in isopropanol. Peptide clean-up was performed using SDB-RPS stage tips (Sigma-Aldrich). Peptides were added to stage tips and washed first with 1% TFA in isopropanol and then with 0.2% TFA in water. Lastly, peptides were eluted in 80% acetonitrile plus 1.25% ammonia and dried in vacuum concentrator.

Mass spectrometry data acquisition (co-immunoprecipitation)

Dried peptides were resuspended in 2%ACN with 0.1% TFA and used for LC-MS² analysis on a QExactive HF mass spectrometer coupled to an easy nLC 1200 (Thermo Fisher Scientific) fitted with a 35 cm long, 75μm ID fused-silica column packed in house with 1.9 μm C18 particles (Reprosil pur, Dr. Maisch). The column was maintained at 40 °C using an integrated column oven (Sonation). Peptides were eluted in a non-linear gradient of 5–40% acetonitrile over 60 min and sprayed into the mass spectrometer equipped with a nanoFlex ion source (Thermo Fisher Scientific). Full-scan MS spectra (300–1,650 m/z) were acquired in profile mode at a resolution of 60,000 at m/z 200, a maximum injection time of 20 m and an AGC (automatic gain control) target value of 3×10^6 . Up to 10 of the most intense peptides per full scan were isolated using a 1.4-Th window for fragmentation by higher energy collisional dissociation (normalized collision energy of 27). MS/MS spectra were acquired in centroid mode with a resolution of 30,000, a maximum injection time of 54 m and an AGC target value of 1×10^5 . Single charged ions, ions with a charge state of more than seven and ions with unassigned charge states were not considered for fragmentation, and dynamic exclusion was set to 20 s to minimize the acquisition of fragment spectra representing already acquired precursors.

Mass spectrometry data analysis (co-IP)

MS raw data were analyzed using FragPipe v21.1, with MSFragger v.4.0⁴⁴ and Philosopher v.5.1.0.⁴⁵ The built-in workflow “LFQ-MBR” was used with a precursor mass tolerance of 20 ppm and fragment mass tolerance of 20 ppm. The human proteome database used by FP (ID: UP000005640, 27/06/2024) comprised of 20,468 reviewed sequences only and their corresponding decoys, including common contaminant proteins. Identifications were filtered to obtain false discovery rates (FDR) below 1% for both peptide spectrum matches (minimum peptide length of 7) and proteins using a target-decoy strategy. For all searches, carbamidomethylated cysteine was set as a fixed modification and oxidation of methionine and N-terminal protein acetylation as variable modifications with allowing up to 3 modifications per peptide. Strict trypsin cleavage was set as protein digestion rule. Label-free quantification was performed using IonQuant v.1.10.27.⁴⁶ Data were further processed using FragPipe Analyst.⁴⁷ Subsequently, the data were plotted in R using custom scripts.

CRBN-focused library

All compounds for the CRBN-focused library were obtained at Enamine using in-house developed procedures. 4480 compounds (10 μL of 10 mM DMSO solutions) were delivered in 384-well echo plates (14 plates), prepared using Labcyte #LP-0200, (320 compounds per plate, first two and last two columns empty).

QUANTIFICATION AND STATISTICAL ANALYSIS

For binding and degradation curves, statistical analysis was conducted using either GraphPad Prism 10 non-linear regression curve fit or normalization and calculation performed with Genedata Analyzer (Gene data, Switzerland). A minimum of $n = 2$ biological replicates were used for each treatment condition. Values are reported as mean and \pm SD, where appropriate. For FP binding screen a Z prime score was calculated to measure quality of the screen and 3-fold the standard deviation was used to determine statistical significance of hits. All proteomics experiments were performed with a minimum of $n = 3$ biological replicates. Statistical analysis was carried out within the R framework and hits were selected based on a set significance threshold (fold-change above 2 and $\log_{10} p$ value below 0.001). Exact n values are reported for individual experiments in figure legends and STAR [method details](#).